



Inhibitory glycinergic neurotransmission in the mammalian auditory brainstem upon prolonged stimulation: short-term plasticity and synaptic reliability

Florian Kramer¹, Désirée Griesemer¹, Dennis Bakker¹, Sina Brill¹, Jürgen Franke^{2,3}, Erik Frotscher¹ and Eckhard Friauf^{1,3*}

¹ Animal Physiology Group, Department of Biology, University of Kaiserslautern, Kaiserslautern, Germany

² Chair for Applied Mathematical Statistics, Department of Mathematics, University of Kaiserslautern, Kaiserslautern, Germany

³ Center for Mathematical and Computational Modeling, University of Kaiserslautern, Kaiserslautern, Germany

Edited by:

Conny Kopp-Scheinflug,
Ludwig-Maximilians-University
Munich, Germany

Reviewed by:

Achim Klug, University of Colorado,
USA

Vibhakar Kotak, New York
University, USA

*Correspondence:

Eckhard Friauf, Animal Physiology
Group, Department of Biology,
University of Kaiserslautern,
POB 3049, D-67653 Kaiserslautern,
Germany
e-mail: eckhard.friauf@
biologie.uni-kl.de

Short-term plasticity plays a key role in synaptic transmission and has been extensively investigated for excitatory synapses. Much less is known about inhibitory synapses. Here we analyze the performance of glycinergic connections between the medial nucleus of the trapezoid body (MNTB) and the lateral superior olive (LSO) in the auditory brainstem, where high spike rates as well as fast and precise neurotransmission are hallmarks. Analysis was performed in acute mouse slices shortly after hearing onset (postnatal day (P)11) and 8 days later (P19). Stimulation was done at 37°C with 1–400 Hz for 40 s. Moreover, in a novel approach named marathon experiments, a very prolonged stimulation protocol was employed, comprising 10 trials of 1-min challenge and 1-min recovery periods at 50 and 1 Hz, respectively, thus lasting up to 20 min and amounting to >30,000 stimulus pulses. IPSC peak amplitudes displayed short-term depression (STD) and synaptic attenuation in a frequency-dependent manner. No facilitation was observed. STD in the MNTB-LSO connections was less pronounced than reported in the upstream calyx of Held-MNTB connections. At P11, the STD level and the failure rate were slightly lower within the ms-to-s range than at P19. During prolonged stimulation periods lasting 40 s, P19 connections sustained virtually failure-free transmission up to frequencies of 100 Hz, whereas P11 connections did so only up to 50 Hz. In marathon experiments, P11 synapses recuperated reproducibly from synaptic attenuation during all recovery periods, demonstrating a robust synaptic machinery at hearing onset. At 26°C, transmission was severely impaired and comprised abnormally high amplitudes after minutes of silence, indicative of imprecisely regulated vesicle pools. Our study takes a fresh look at synaptic plasticity and stability by extending conventional stimulus periods in the ms-to-s range to minutes. It also provides a framework for future analyses of synaptic plasticity.

Keywords: synaptic fidelity, fast-spiking cells, short-term depression, inhibitory postsynaptic currents, synaptic attenuation, lateral superior olive, medial nucleus of the trapezoid body, high-frequency neurotransmission

INTRODUCTION

Fast and reliable synaptic transmission at high frequencies is one of the hallmarks of the auditory system. In particular, it is a key feature for processing interaural time and intensity differences, the two major features for computation of sound localization (reviews: Yin, 2002; Borst and Soria van Hoeve, 2012). Central auditory relay synapses can follow high-frequency inputs (>100 Hz) with great fidelity, conveying signals with a high degree of precision and reliability (review: Klug, 2011). A great deal of knowledge concerning synaptic transmission has been obtained from principal neurons in the medial nucleus of the trapezoid body (MNTB) and their giant presynaptic partner structure, the calyx of Held, between which phase-locked transmission occurs in a failure-free, one-to-one fashion up to a frequency of 800 Hz, at least over a short period of 20 ms (Taschenberger and von Gersdorff, 2000). MNTB neurons provide the major inhibitory input to neurons in the lateral superior

olive (LSO), and the MNTB-LSO pathway is a model system for investigating inhibitory neurotransmission (Sanes and Friauf, 2000; Kandler, 2004; Noh et al., 2010). In contrast to the well-characterized calyx of Held-MNTB synapses, however, much less is known about the reliability of downstream MNTB-LSO synapses.

Despite the demands concerning stable signal transmission, synapses display substantial, mostly temporary, alterations in strength during repetitive use. Distinctive types of synaptic plasticity are exhibited, such as depression and facilitation, or combinations of both. In the auditory system, calyceal input to MNTB neurons has been extensively analyzed (von Gersdorff et al., 1997; Taschenberger and von Gersdorff, 2000; Taschenberger et al., 2002; Trussell, 2002; von Gersdorff and Borst, 2002; Wong et al., 2003; Oleskevich et al., 2004). By contrast, in other auditory relay stations, short-term alterations are relatively unexplored (reviews: Bender and Trussell, 2011; MacLeod, 2011).

Short-term depression (STD) in a brief time window of <1 s has been described at specialized terminals of auditory nerve fibers, the endbulbs of Held, which contact bushy cells in the cochlear nuclear complex. Here, STD occurs upon stimulation with 100–300 Hz over a period of 150 ms (Oleskevich and Walmsley, 2002; Wang and Manis, 2006, 2008; Wang et al., 2010, 2011). STD was also reported in GABAergic synapses between the inferior colliculus and the medial geniculate body (Venkataraman and Bartlett, 2013). In the auditory cortex, GABAergic IPSCs display STD in a layer-specific manner (Humberto et al., 2011). In the only LSO studies so far, STD in the inhibitory MNTB-LSO path was described in P11–15 mice at 23–25°C with stimulus trains of 20 Hz lasting 1.05 s (Giugovaz-Tropper et al., 2011) and in P10–18 gerbils and P10–15 mice at 32°C with stimulus trains of 100 Hz lasting 200 ms (Walcher et al., 2011).

Here, we have functionally analyzed glycinergic MNTB-LSO synapses with the aims to characterize their performance and to determine their limits. To do so, IPSCs were recorded from mouse LSO neurons in brainstem slices at two ages (P11 and P19), two temperatures (37 and 26°C), and various frequencies (1–400 Hz). Moreover, “marathon experiments” involved very prolonged stimulation (20 min) comprising up to 30,600 stimuli, many-fold more than routinely used (cf. Galarreta and Hestrin, 1998). The rationale for this strategy is based on several arguments. First, continuous auditory stimulation is virtually ubiquitous in natural environments (Lalor et al., 2009). Second, brief tone bursts, commonly used stimuli for *in vivo* recordings, recruit bursts of action potentials (APs) at frequencies between 50 and 500 Hz (Klug, 2011). Finally, highly active conditions of prolonged stimulation are a better approximation of the *in vivo* situation than standard slice experiments. Our novel stimulus protocols address synaptic depression in both the milliseconds-to-seconds (STD) and the tens of seconds-to-minute range, for which we use the term “synaptic attenuation” as the counterpart to the term synaptic augmentation (Thompson, 2000; Regehr, 2012). Concerning the mechanisms underlying STD and synaptic attenuation, we provide some evidence in favor of presynaptic processes.

MATERIALS AND METHODS

ANIMALS

Experiments were performed on C57BL/6N mice of either sex at postnatal day (P)11 \pm 1 or P19 \pm 1. They were in accordance with the German law for conducting animal experiments and followed the NIH guide for the care and use of laboratory animals.

ELECTROPHYSIOLOGY

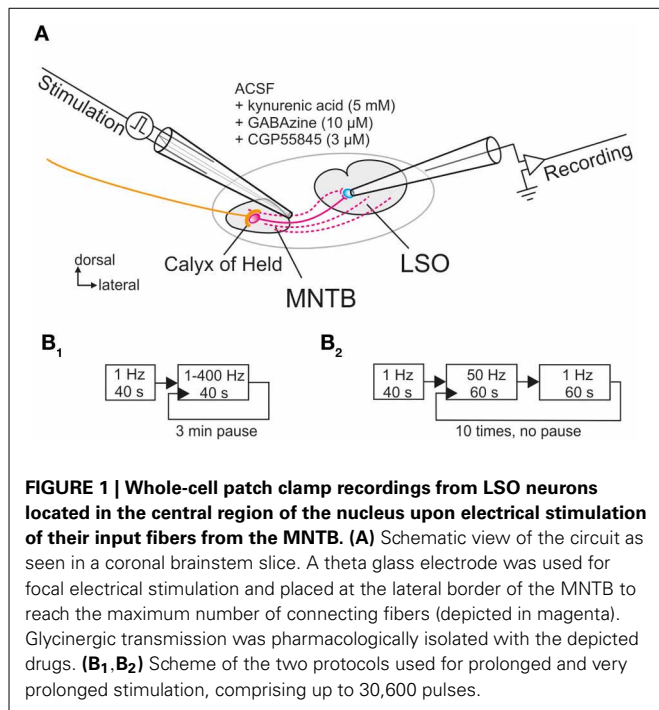
Patch-clamp recordings from LSO neurons were performed in the whole-cell configuration in acute brainstem slices generated as described previously (Balakrishnan et al., 2003). Slices were stored at room temperature in artificial cerebrospinal fluid (ACSF, in [mM]: NaCl 125; KCl 2.5; NaHCO₃ 25; NaH₂PO₄ 1.25; Na-pyruvate 2; D-glucose 10; CaCl₂ 2; MgCl₂ 1; myo-inositol 3; ascorbic acid 0.44; pH = 7.3 when bubbled with 95% O₂-5% CO₂) before being transferred into a recording chamber in which they were continually superfused with ACSF (1–2 ml/min). Recordings were performed at near physiological temperature

(37 \pm 1°C, temperature controller III, Luigs&Neumann) or at room temperature (26 \pm 2°C). The recording chamber was mounted on an upright microscope (Eclipse E600FN, Nikon) equipped with differential interference contrast optics (4 \times CFI Achromate, 0.1 NA; 60 \times CFI Fluor W, 1.0 NA, Nikon) and an infrared video camera system (CCD camera C5405-01, Hamamatsu). LSO principal neurons were identified by their location in the center of the nucleus, orientation, size, spindle-shaped somata, the presence of hyperpolarization-activated inward currents (Sterenberg et al., 2010) and of short-latency IPSCs upon stimulation of MNTB fibers. Membrane currents were digitized and stored using ClampEX 8.2 (Molecular Devices).

Patch pipettes were pulled from borosilicate glass capillaries (GB150(F)-8P, Science Products) with a horizontal puller (P-87, Sutter Instruments). They were connected to an Axopatch-1D patch-clamp amplifier (Molecular Devices) and had resistances of 3–7 M Ω when filled with intracellular solution (in [mM]: HEPES 10; EGTA 5; MgCl₂ 1; K-gluconate 140; Na₂ATP 2; Na₂GTP 0.3). The Cl⁻ concentration of 2 mM was slightly lower than the native 5 mM previously determined for P9–11 via perforated-patch clamp recordings (Ehrlich et al., 1999) and was chosen to increase the driving force for inward-directed Cl⁻ flow. With 2 mM [Cl⁻]_i, E_{Cl} was -112 mV at 37°C and -108 mV at 26°C. Liquid junction potential was calculated using the program JPCalc (Barry, 1994); it amounted to 15.4 mV and was corrected offline. Data were sampled at 10 kHz, low-pass filtered at 5 kHz, and analyzed using ClampEX and ClampFit 8.2.0.235 (Molecular Devices) and Origin software (Origin Lab). Capacitive current transients were electronically compensated online, and the whole cell capacitance was estimated from this compensation. Throughout the experiments, the series resistance was monitored and ranged from 6 to 20 M Ω . It was routinely compensated by 60–80%. If it exceeded 20 M Ω , recordings were excluded from further analysis.

Recordings were performed in voltage clamp mode at a holding potential of -70 mV. To evoke inhibitory postsynaptic currents (IPSCs), a theta glass electrode (TST150-6, WPI) with a tip diameter of 10–20 μ m was filled with ACSF and placed lateral to the MNTB (Figure 1A). Monopolar pulses (100 μ s duration) were applied through a programmable pulse generator (Master 8, A.M.P.I.) connected to a stimulus isolator unit (A360, WPI). The amplitude of the stimulus pulses ranged from 0.1 to 4 mA and was set to achieve stable synaptic responses with a jitter in amplitude of <50 pA.

For normalization, 40 control stimuli were presented at 1 Hz during a baseline period and the peak amplitudes of the 40 IPSCs were averaged (= control value, set to 100%; cf. Galarreta and Hestrin, 1998). Two protocols were employed for determining the synaptic performance of the MNTB-LSO connection. For protocol 1, pulse trains were applied for 40 s each, with stimulation frequencies from 1 to 400 Hz in random order, and a 3-min pause was introduced between each pulse train (Figure 1B₁). For protocol 2, which assessed the performance over 20 min, 10 trials of stimulation were applied, alternating between 50 Hz stimulation for 60 s and 1 Hz stimulation for another 60 s (Figure 1B₂). 1 Hz stimulation for 60 s was chosen to describe the time course of recovery, rather than eliciting single test IPSCs at varying



time intervals (Giugovaz-Tropper et al., 2011). No pause was introduced between trials. In some control experiments, recordings were obtained from MNTB neurons in the current-clamp mode, and antidromic APs were evoked in the LSO by electrical stimulation of MNTB axons.

CHEMICALS AND PHARMACOLOGICAL COMPOUNDS

All chemicals were purchased from Sigma-Aldrich unless stated otherwise. Glycine-mediated receptor currents were isolated pharmacologically. To do so, N-methyl-D-aspartic acid (NMDA) and α -amino-3-hydroxy-5-methyl-4-isoxazole propionate (AMPA) receptor-mediated currents were blocked by kynurenic acid (5 mM). Furthermore, GABAzine (10 μ M) and CGP55845 (3 μ M) were used for blocking GABA_A and GABA_B receptor-mediated currents, respectively (purchased from Ascent Scientific and Tocris Bioscience). All drugs were added to the ACSF. In control experiments, the residual current could be completely abolished with strychnine (0.3 – 1 μ M), thus verifying their glycinergic nature.

DATA ANALYSIS

Data analysis was performed with Mini Analysis 6.0.3 (Synaptosoft). At the beginning of each experiment, the control value of glycinergic IPSC peak amplitudes was obtained for each neuron (see above). The following peak amplitudes underwent statistical analysis: amplitudes of the 1st, 2nd, and 10th IPSC (IPSC₁, IPSC₂, IPSC₁₀), amplitudes after the 1st and the 40th s (IPSC_{1s}, IPSC_{40s}), and averaged amplitudes over several 10-s periods, namely 30–40 s, 50–60 s, and 110–120 s (IPSC_{30–40s}, IPSC_{50–60s}, IPSC_{110–120s}). When individual IPSC peak amplitudes were $\leq 5\%$ of the control value, the event was considered a failure. A failure was also attributed if the peak amplitude was < 15 pA, which equaled the noise level. For

such failures, the peak amplitude was set to 0 pA. For kinetic measurements, the decay time constant τ (decay to 37% of peak amplitude) was determined by fitting a single exponential to the decay phase of the IPSC.

STATISTICS

Statistical analysis was performed on data sets if $n \geq 7$ (Winstat, R. Fitch Software). Outliers (more than four times standard deviation above/below mean) were excluded. Such outliers occurred in the range of 5.3–11.8% (median: 6.2%, mean: 8.0%). In absolute numbers, $n_{\text{gross}} = 19$ became $n_{\text{net}} = 18$ in the best case, and $n_{\text{gross}} = 17$ became $n_{\text{net}} = 15$ in the worst case. Samples with a Gaussian distribution (Kolmogorov–Smirnov) were compared using a paired or an unpaired two-tailed Student's *t*-test. A Wilcoxon-signed rank test was used for unequal variances. Equality of variances in unpaired samples Student's *t*-tests was assessed with an *F*-test. Values in bar charts are presented as mean \pm s.e.m. Significance values were as follows: * $p < 0.05$, ** $p < 0.01$, *** $p < 0.001$.

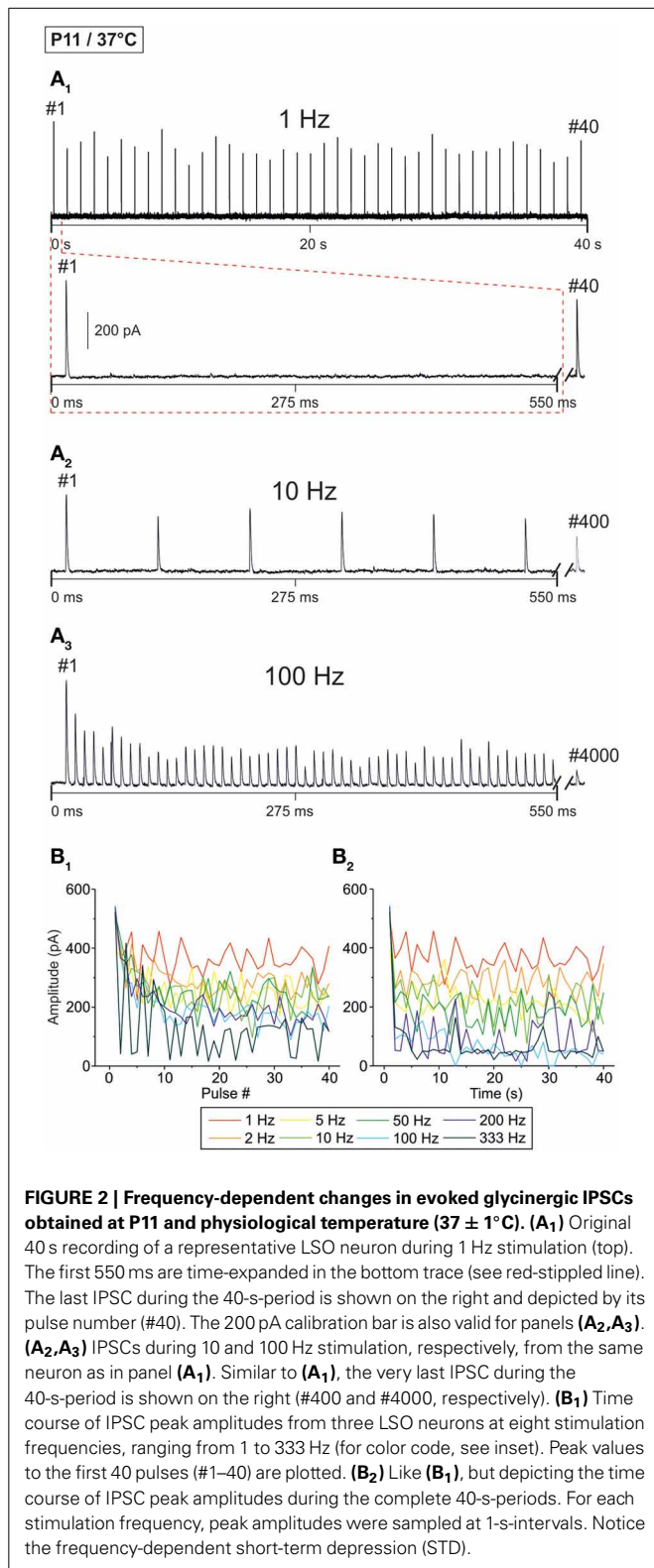
RESULTS

FREQUENCY-DEPENDENT SYNAPTIC DEPRESSION OF GLYCINERGIC IPSCs IN THE MILLISECONDS-TO-SECONDS RANGE

In a first series of experiments, synaptic current responses from LSO principal neurons were obtained by stimulating axons in the MNTB at P11, and glycinergic IPSCs were pharmacologically isolated at a holding potential of -70 mV (Figure 1A). Under these conditions, IPSCs comprised outward currents with a fast rising phase (< 1 ms) and short decay times (< 5 ms), corroborating that they were mediated through glycine receptors (GlyRs). The performance of the glycinergic MNTB-LSO synapses was assessed by prolonged stimulation for 40 s with frequencies of 1–400 Hz (in random order), inserting a 3-min pause in between (Figure 1B₁). As spontaneous discharges in this frequency and time range have been described for mouse MNTB neurons *in vivo* at P11–12 and thereafter (Sonntag et al., 2009), our stimuli resembled physiological conditions. We were further motivated to stimulate the MNTB-LSO synapses for prolonged periods with 1–400 Hz because mean spontaneous firing rates in this domain (25–100 Hz) have been recorded *in vivo* from auditory nerve fibers in several species, such as cats (Liberman, 1978), gerbils (Hermann et al., 2007), and chinchillas (Temchin et al., 2008).

Representative current traces from a P11 LSO neuron at $37 \pm 1^\circ\text{C}$ are illustrated in Figure 2A. At 1 Hz, every stimulus pulse elicited an IPSC (Figures 2A₁, B₁). As the stimulus frequency was increased, IPSC peak amplitudes declined, resulting in STD (Figures 2A₂–B₁). There was no indication of a short-term facilitation. Despite the frequency-dependent STD, the neuron displayed a detectable IPSC to each of the first 40 stimulus pulses, even at 333 Hz. STD was most prominent during the first 10 pulses (Figure 2B₁), whereas the peak amplitudes appeared to be quite stable after 5 s (Figure 2B₂). With time, however, some pulses remained unresponded, i.e., failures occurred (Figure 2B₂, five values at 100 Hz touching x axis after > 10 s).

The STD behavior shown exemplarily in Figure 2 was observed in the whole ensemble of P11/37°C LSO neurons



($n = 4\text{--}22$, depending on stimulus frequency; **Figure 3**). At each stimulus frequency and for virtually every neuron, the first IPSC (IPSC₁) had the highest peak amplitude (**Figure 3A**, see Methods for normalization to 100%). This was quantified by

calculating the ratio between the mean peak amplitude of IPSC₂ and IPSC₁ (IPSC₂/IPSC₁). For example, at 1, 10, and 100 Hz, IPSC₂/IPSC₁ ratios amounted to 0.84, 0.85, and 0.80, respectively (**Table 1** and **Figure 3B₁**). After the initial decline between IPSC₁ and IPSC₂, STD continued during the first 10 pulses, such that IPSC₁₀ was of significantly lower peak amplitude than IPSC₂ at stimulus frequencies ≥ 2 Hz (e.g., IPSC₁₀/IPSC₂ ratio at 50 Hz: 0.59; **Table 1**, **Figure 3B₁**). Because of the prolonged stimulation period of 40 s, we extended the quantification from a pulse-based to a time-based analysis. During the first second of stimulation, peak amplitudes declined significantly and in a frequency-dependent manner >2 Hz (e.g., IPSC_{1s}/IPSC₂ at 50 Hz: 0.54; **Table 1**, **Figure 3B₂**). No further decline occurred between IPSC_{1s} and IPSC_{40s}, except for stimulus frequencies of 50 and 100 Hz, implying that stable inhibitory response amplitudes are maintained in the seconds-to-minutes range up to 10 Hz at P11/37°C (**Table 1**).

The frequency-dependent depression behavior was also evident in the mean peak amplitudes obtained during the last 10 s of recording, when a steady-state scenario appeared to be present (30–40 s; **Figures 3B₂, C**). Peak amplitudes declined significantly with stimulus frequency up to 100 Hz, with no further decline at higher frequencies. The low mean amplitudes ($<10\%$ of the control) at ≥ 100 Hz are indicative of a massive depression in the P11/37°C MNTB-LSO connections in the seconds-to-minute range when the stimulus frequency is >50 Hz (**Figures 3B₂, C**).

Concomitant with the frequency-dependent decline of peak amplitudes, LSO neurons were not able to respond reliably (i.e., failure-free) to high frequency stimulation, even during the first 40 pulses (**Table 2**, **Figures 3A₁–A₈**). Virtually 100% fidelity (no failures) was observed up to 50 Hz, because only a single failure occurred in a total of 2840 events, namely at 10 Hz (**Figure 3A₄**). At 100 Hz, however, 27% of the neurons (4 of 15) displayed failures, and the average failure rate amounted to 0.8% (5 failures in 600 events), still a low value (**Figure 3A₆**). The effect became more pronounced at even higher frequencies (333 Hz: 16.3% failure rate, 26 failures in 160 events, 3 of 4 neurons, **Figure 3A₈**, **Table 2**). When analyzing the failure rate during the last 40 pulses, 100% fidelity was present only up to a stimulus frequency of 10 Hz (**Table 2**). At 50 Hz, 46% of the neurons (10 of 22) displayed failures with an average failure rate of 21% (188 failures in 880 events). Both the number of neurons with failures and the failure rate increased with stimulus frequency. Every neuron displayed failures at ≥ 100 Hz, and at 333 Hz, the failure rate amounted to 89.4% (**Table 2**). In summary, 50 Hz appears to be the maximal stimulus frequency to which P11/37°C MNTB-LSO synapses can continually respond within a time frame of milliseconds to tens of seconds.

TEMPERATURE-DEPENDENCY OF STD IN THE MILLISECONDS-TO-SECONDS RANGE

Next, we analyzed temperature effects on synaptic transmission. To do so, P11 LSO principal neurons were analyzed as described above, yet recordings were obtained at $26 \pm 2^\circ\text{C}$. Representative recordings are illustrated in **Figure 4A**. Similar to the scenario at 37°C, IPSCs were reliably evoked at 1 Hz (**Figure 4A₁**). IPSC amplitudes declined when the interpulse interval was shortened,

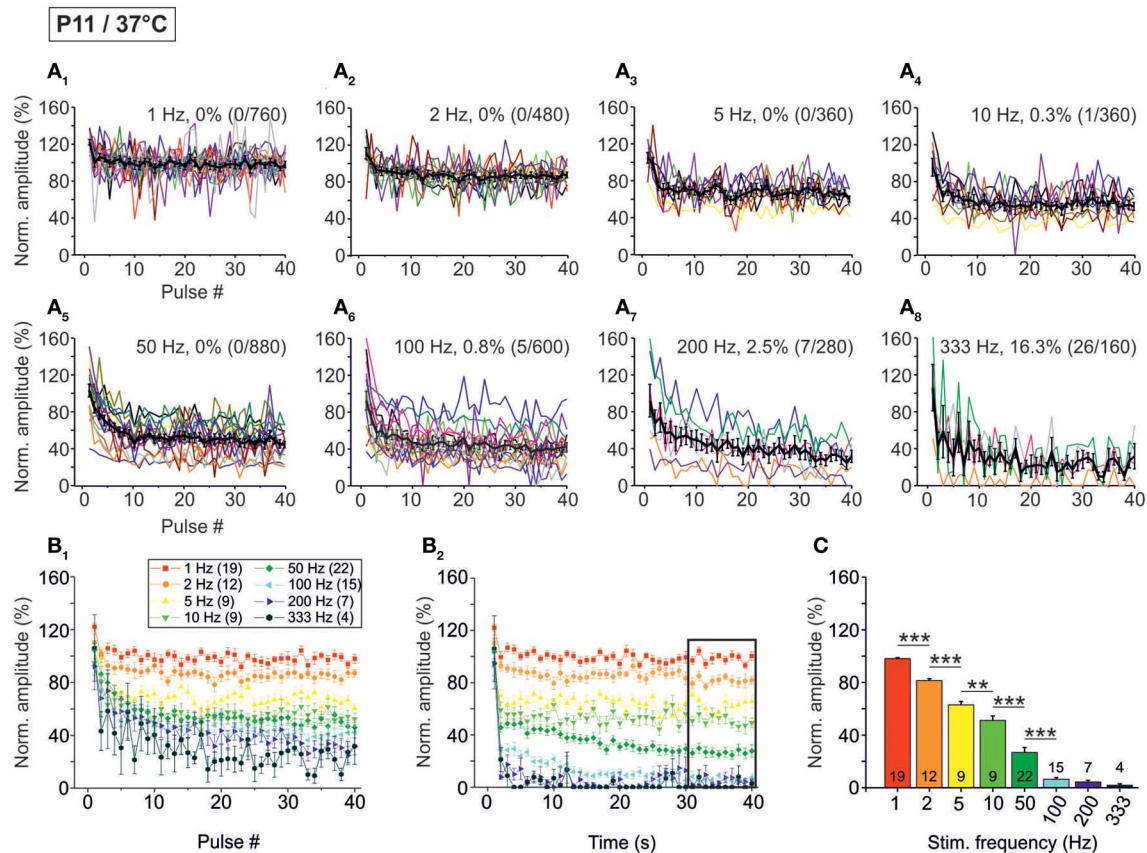


FIGURE 3 | Population data illustrating the frequency-dependent time course of glycinergic IPSC peak amplitudes at P11/37°C. (A₁–A₈)

Color-coded plots for all recorded LSO neurons at eight stimulation frequencies ($n = 4$ –22, cf. inset in panel **B₁**), depicting the time course of IPSC amplitudes in response to the first 40 stimuli. In each panel, the mean values \pm s.e.m. are shown in black. The failure rate (%) and the ratio failures/events across neurons are also provided in each panel. **(B₁)** Mean values \pm s.e.m. of the first 40 IPSCs obtained in response to the eight

different stimulation frequencies. Notice the decline to $<40\%$ at frequencies ≥ 100 Hz. **(B₂)** Mean values \pm s.e.m. obtained during the complete 40-s-periods of stimulation (sampled at 1-s-intervals). Color code as in panel **(B₁)**. Notice the decline to $<20\%$ at frequencies ≥ 100 Hz. Black frame frame depicts the last 10 data points in each trace that underwent statistical analysis shown in panel **(C)**. **(C)** IPSC peak amplitudes decreased with increasing stimulation frequency. N numbers in the inset of **(B₁)** correspond to all panels. $**p < 0.01$; $***p < 0.001$.

yet IPSC₁ to IPSC₄₀ were evoked reliably, even at a stimulus frequency of 200 Hz (**Figures 4A₂–B₁**). However, prolonged stimulation (40 s) resulted in drastically reduced peak amplitudes after 5 s at stimulus frequencies ≥ 50 Hz, and many failures occurred at 100 and 200 Hz (**Figure 4B₂**). Since the IPSCs decay time was >3 ms at 26°C (cf. **Figure 8**), we refrained from performing experiments with stimulus frequencies ≥ 333 Hz.

The analysis across the ensemble of P11/26°C LSO neurons ($n = 4$ –18) revealed similarities as well as differences in STD behavior compared to 37°C (**Figure 5**). Similarly to 37°C, the mean IPSC₂ amplitude was significantly lower than the IPSC₁ amplitude at each frequency, with IPSC₂/IPSC₁ ratios amounting to 0.88, 0.69, and 0.61 at 1, 10, and 100 Hz, respectively (**Table 1**). Also similarly, further depression occurred from IPSC₂ to IPSC₁₀ (e.g., IPSC₁₀/IPSC₂ ratio at 50 Hz: 0.61; **Table 1**, **Figure 5B₁**), and the amount of depression was generally higher than at 37°C. The most prominent difference between 26 and 37°C became obvious only upon prolonged stimulation. For example at 100 Hz, the decline of peak amplitudes between IPSC₂ and

IPSC₁₅ (obtained after 1 s) was more pronounced at 26°C than at 37°C (IPSC₁₅/IPSC₂ ratio: 0.24 vs. 0.39). The greater reduction with time at lower temperature was corroborated by the IPSC_{40s}/IPSC_{1s} ratios. For example at 50 Hz, the ratio was 0.07 at 26°C, yet 0.61 at 37°C (**Table 1**). In line with this, the mean peak amplitudes obtained within 30–40 s at 50 Hz/26°C were drastically lower than those at 10 Hz/26°C, and there was no further decline beyond 50 Hz (**Figures 5B₂,C**). Together, a major temperature effect is that MNTB-LSO synapses can continually respond to 50 Hz stimulation at 37°C, yet only up to 10 Hz at 26°C.

Concerning the failure rate, P11/26°C MNTB-LSO synapses were able to respond with 100% fidelity to the first 40 pulses only up to a frequency of 5 Hz, because at 10 Hz, 1.1% failures occurred in 2 of 11 neurons (5 of 440 events; **Figures 5A₁–A₄**, **Table 2**). This was again in contrast to 37°C (0.3% failures) and further emphasized by a more than 10-fold higher failure rate at 100 Hz (26°C: 8.3%; 37°C: 0.8%, **Figure 5A₆**, **Table 2**). During the last 40 pulses, 100% fidelity was present only up to 5 Hz. Above 10 Hz, each neuron displayed failures, with a striking

Table 1 | Frequency-dependent changes in glycinergic IPSCs evoked in the MNTB-LSO connections.

Stimulus frequency (Hz)	n	IPSC ₁ (%)	IPSC ₂ (%)	IPSC ₁₀ (%)	IPSC _{1s} (%)	IPSC _{40s} (%)	IPSC _{30-40s} (%)	IPSC ₂ /IPSC ₁ [P]	IPSC ₁₀ /IPSC ₂ [P]	IPSC _{1s} /IPSC ₂ [P]	IPSC _{40s} /IPSC _{1s} [P]
P11/37°C											
1	19	122.1 ± 2.6	103.0 ± 2.6	99.3 ± 3.0	103.0 ± 2.6	100.4 ± 3.3	98.2 ± 0.6	0.84 [8E-06]	0.96 [0.449]	n.d.	1.0 [0.477]
2	12	110.5 ± 6.1	99.5 ± 1.9	92.7 ± 4.7	92.7 ± 3.7	83.6 ± 2.1	81.6 ± 1.3	0.90 [0.011]	0.93 [0.029]	0.93 [0.211]	0.90 [0.064]
5	9	104.7 ± 5.7	93.4 ± 4.6	71.1 ± 6.4	69.9 ± 4.5	65.4 ± 4.7	62.9 ± 2.6	0.89 [0.012]	0.76 [0.008]	0.75 [0.002]	0.94 [0.287]
10	9	94.9 ± 9.6	80.3 ± 6.5	53.2 ± 4.5	59.2 ± 5.7	49.4 ± 3.6	51.1 ± 3.0	0.85 [0.035]	0.66 [8E-04]	0.74 [0.005]	0.83 [0.089]
50	22	100.2 ± 5.1	83.9 ± 4.6	49.4 ± 3.2	45.6 ± 3.4	27.7 ± 4.8	26.8 ± 3.8	0.84 [5E-05]	0.59 [3E-08]	0.54 [2E-06]	0.61 [0.001]
100	15	92.1 ± 10.1	73.6 ± 7.5	46.5 ± 5.3	28.5 ± 4.6	7.5 ± 2.6	6.5 ± 1.3	0.80 [0.004]	0.63 [8E-04]	0.39 [1E-04]	0.26 [0.004]
200	7	94.6 ± 19.3	68.0 ± 14.0	49.2 ± 11.0	7.8 ± 1.5	3.6 ± 2.8	4.3 ± 1.3	0.72	0.72	0.11	0.46
333	4	106.1 ± 25.1	43.3 ± 14.6	40.4 ± 14.1	21.2 ± 9.2	2.8 ± 2.8	1.9 ± 1.0	0.41	0.93	0.49	0.13
P11/26°C											
1	11	140.2 ± 7.5	124.0 ± 3.3	100.0 ± 2.4	124.0 ± 3.3	99.2 ± 2.3	96.2 ± 1.5	0.88 [0.005]	0.81 [1E-05]	n.d.	0.80 [1E-06]
2	11	149.8 ± 5.6	119.1 ± 6.4	79.7 ± 6.6	94.6 ± 3.6	78.3 ± 4.7	78.3 ± 2.3	0.80 [0.012]	0.67 [3E-06]	0.79 [0.006]	0.83 [0.022]
5	11	147.1 ± 4.2	106.3 ± 5.9	62.4 ± 5.2	74.6 ± 4.6	69.1 ± 5.0	63.6 ± 3.8	0.72 [7E-05]	0.59 [2E-04]	0.70 [0.003]	0.93 [0.018]
10	11	163.0 ± 16.6	112.2 ± 11.6	71.1 ± 7.4	69.7 ± 6.9	47.3 ± 6.9	49.9 ± 4.5	0.69 [1E-05]	0.63 [3E-04]	0.62 [2E-04]	0.68 [0.014]
50	17	133.5 ± 6.7	113.7 ± 6.6	69.2 ± 8.2	40.7 ± 5.5	2.9 ± 1.4	2.2 ± 0.6	0.85 [0.027]	0.61 [1E-04]	0.36 [2E-08]	0.07 [2E-06]
100	18	133.8 ± 17.5	81.7 ± 10.7	40.4 ± 5.2	19.6 ± 3.3	0.0 ± 0.0	1.4 ± 0.5	0.61 [0.005]	0.49 [7E-04]	0.24 [1E-06]	0.00 [2E-04]
200	4	110.5 ± 30.0	48.6 ± 10.1	24.6 ± 6.6	5.5 ± 3.2	3.9 ± 2.7	1.3 ± 0.9	0.44	0.51	0.11	0.71
P19/37°C											
1	13	125.9 ± 6.7	101.6 ± 6.5	99.0 ± 7.7	101.6 ± 6.5	94.7 ± 5.7	99.7 ± 1.9	0.81 [0.063]	0.97 [0.790]	n.d.	0.93 [0.486]
2	12	111.8 ± 5.8	92.0 ± 7.5	72.0 ± 4.6	78.9 ± 7.7	72.9 ± 4.7	71.5 ± 3.7	0.82 [0.033]	0.76 [0.057]	0.86 [0.295]	0.92 [0.550]
5	12	93.9 ± 8.7	74.3 ± 7.6	60.6 ± 9.4	68.1 ± 6.8	56.5 ± 4.8	57.3 ± 3.8	0.79 [0.005]	0.82 [0.267]	0.92 [0.541]	0.83 [0.186]
10	11	101.0 ± 6.8	78.3 ± 7.1	42.8 ± 6.5	41.5 ± 4.3	64.6 ± 8.7	54.4 ± 3.0	0.78 [0.006]	0.55 [0.002]	0.53 [1E-04]	1.56 [0.055]
50	11	84.2 ± 8.7	72.9 ± 9.4	37.1 ± 5.5	33.2 ± 4.6	40.4 ± 7.5	36.1 ± 3.7	0.87 [0.156]	0.51 [0.001]	0.46 [2E-04]	1.21 [0.318]
100	15	88.2 ± 7.3	75.5 ± 9.6	44.8 ± 5.3	39.8 ± 7.5	21.0 ± 5.9	28.7 ± 5.2	0.86 [0.096]	0.59 [0.003]	0.53 [0.010]	0.53 [0.001]
200	8	96.2 ± 18.1	79.0 ± 9.5	49.0 ± 10.9	32.4 ± 8.7	10.2 ± 6.0	6.3 ± 2.7	0.82 [0.233]	0.77 [0.116]	0.86 [0.392]	0.15 [0.010]
333	7	84.9 ± 20.2	44.3 ± 14.3	34.2 ± 11.3	13.5 ± 7.8	0.0 ± 0.0	2.3 ± 1.1	0.52	0.77	0.31	0.00
400	7	83.7 ± 13.0	46.4 ± 18.5	3.7 ± 3.7	6.3 ± 4.3	0.0 ± 0.0	0.9 ± 0.7	0.55	0.08	0.14	0.00

Depicted are the mean values of IPSC peak amplitudes ± s.e.m. in relation to the control amplitude. The control amplitude is the average amplitude obtained for each neuron at the beginning of the experiment upon 40 stimuli at 1 Hz and was set to 100%. Statistical analysis (Student's t-test) was performed only on data sets with $n \geq 8$. $P =$ significance value. Because $IPSC_{1s} = IPSC_2$ at 1 Hz stimulation, the ratio $IPSC_{1s}/IPSC_2$ is meaningless and, therefore, it was not determined at this frequency (n.d.).

Table 2 | Failure analysis of glycinergic IPSCs evoked in the MNTB-LSO connections.

Stimulus frequency (Hz)	P11/37°C			
	First 40 pulses		Last 40 pulses	
	Neurons with failures (%) [ratio]	Failure rate (%) [failures/events]	Neurons with failures (%) [ratio]	Failure rate (%) [failures/events]
1	0 [0/19]	0 [0/760]	0 [0/19]	0 [0/760]
2	0 [0/12]	0 [0/480]	0 [0/12]	0 [0/480]
5	0 [0/9]	0 [0/360]	0 [0/9]	0 [0/360]
10	11 [1/9]	0.3 [1/360]	0 [0/9]	0 [0/360]
50	0 [0/22]	0 [0/880]	46 [10/22]	21.4 [188/880]
100	27 [4/15]	0.8 [5/600]	93 [14/15]	55.5 [333/600]
200	29 [2/7]	2.5 [7/280]	100 [7/7]	71.1 [199/280]
333	75 [3/4]	16.3 [26/160]	100 [4/4]	89.4 [143/160]
P11/26°C				
1	0 [0/11]	0 [0/440]	0 [0/11]	0 [0/440]
2	0 [0/11]	0 [0/440]	0 [0/11]	0 [0/440]
5	0 [0/11]	0 [0/440]	0 [0/11]	0 [0/440]
10	18 [2/11]	1.1 [5/440]	9 [1/11]	3.2 [14/440]
50	12 [2/17]	2.8 [19/680]	100 [17/17]	76.2 [518/680]
100	44 [8/18]	8.3 [60/720]	100 [18/18]	89.4 [644/720]
200	25 [1/4]	12.5 [20/160]	100 [4/4]	100 [160/160]
P19/37°C				
1	0 [0/13]	0 [0/520]	0 [0/13]	0 [0/520]
2	0 [0/12]	0 [0/480]	0 [0/12]	0 [0/480]
5	8 [1/12]	0.2 [1/480]	0 [0/12]	0 [0/480]
10	9 [1/11]	0.2 [1/440]	9 [1/11]	0.2 [1/440]
50	18 [2/11]	0.5 [2/440]	46 [5/11]	4.1 [18/440]
100	40 [6/15]	3.7 [22/600]	60 [9/15]	26.2 [157/600]
200	38 [3/8]	4.1 [13/320]	100 [8/8]	78.4 [251/320]
333	86 [6/7]	28.9 [81/280]	100 [7/7]	93.2 [261/280]
400	100 [7/7]	45.4 [127/280]	100 [7/7]	96.1 [269/280]

Because of the long duration of IPSCs at P11/26°C, stimulus frequencies of 333 and 400 Hz were not applied.

difference to the corresponding failure rates at 37°C (Table 2). Together, these data show that 5–10 Hz is the highest stimulus frequency to which P11/26°C MNTB-LSO synapses can continually respond within a time frame of milliseconds to tens of seconds.

AGE-DEPENDENCY OF STD IN THE MILLISECONDS-TO-SECONDS RANGE

Although synaptic transmission in the rodent MNTB-LSO pathway appears to be quite mature by hearing onset (Kim and Kandler, 2003; Sonntag et al., 2011), some maturation steps still take place thereafter (Sanes and Friauf, 2000; Awatramani et al., 2005). To take this into consideration, we addressed synaptic transmission more than 1 week after hearing onset which, in mice, occurs at about P10 (Mikaelian and Ruben, 1965; Ehret, 1976; Ehret and Romand, 1992). We recorded from P19 LSO principal neurons at 37°C, essentially following the stimulus paradigms described above (highest stimulus frequency: 400 Hz). Figure 6

shows representative data from two neurons. Similar to P11/37°C, amplitudes declined in a time- and frequency-dependent manner.

When analyzing the sample of all LSO neurons ($n = 7-15$), STD was consistently observed, progressing up to 200 Hz (Figure 7, Table 1). In slight contrast to P11/37°C, the mean IPSC₂ peak amplitude was significantly lower than that of IPSC₁ at only three of nine frequencies. For example, at 10 Hz, the IPSC₂/IPSC₁ ratio amounted to 0.78 ($p = 0.006$). At P11/37°C, the corresponding ratio was 0.85. A significant decline between IPSC₂ and IPSC₁₀ did not occur systematically. If there was one, it was moderate (e.g., IPSC₁₀/IPSC₂ at 100 Hz: 0.59; Figure 7B₁, Table 1) and similar to P11/37°C. STD between IPSC₂ and IPSC_{1s} was significant only at ≥ 10 Hz (Figure 7B₂, Table 1). After the first second, peak amplitudes were quite stable and in a steady state, as evidenced by the finding that a statistically significant decline between IPSC_{1s} and IPSC_{40s} was evident only at 100 and 200 Hz (e.g., IPSC_{40s}/IPSC_{1s} at 100 Hz: 0.53; Table 1). Thus, 1–40 s depression at P19 was slightly less pronounced than at

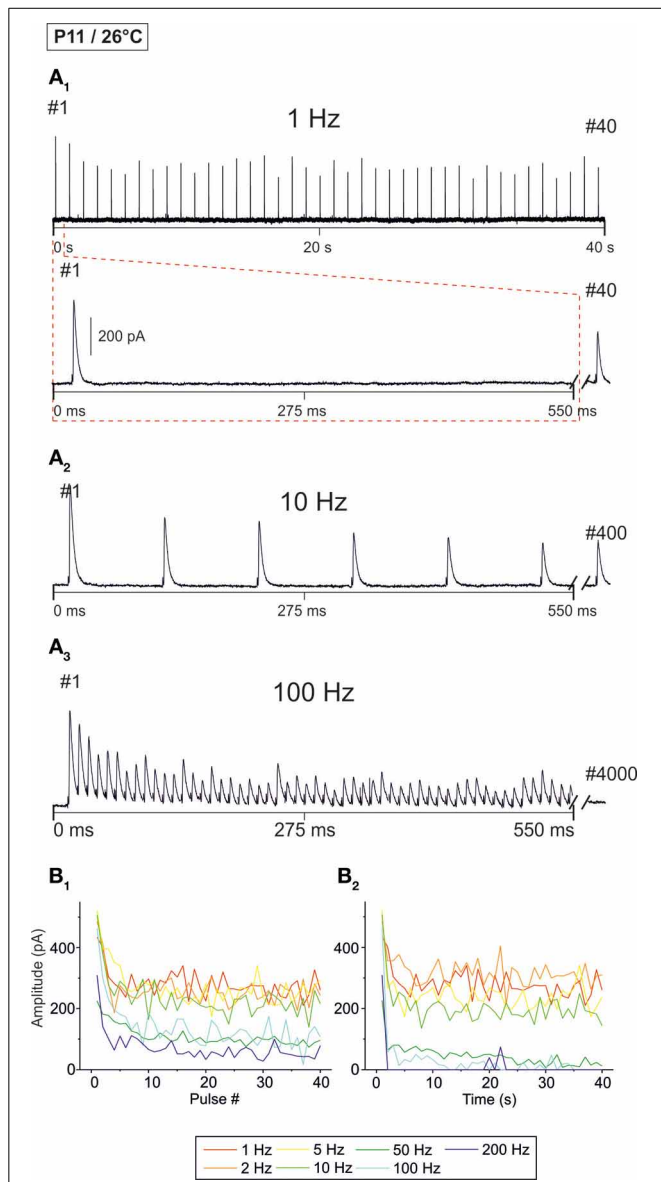


FIGURE 4 | Frequency-dependent changes in evoked glycinergic IPSCs obtained at P11 and room temperature ($26 \pm 2^\circ\text{C}$). (A₁) Original 40 s recording of a representative LSO neuron during 1 Hz stimulation (top). The first 550 ms are time-expanded in the bottom trace (see red-stippled line). The last IPSC during the 40-s-period is shown on the right and depicted by its pulse number (#40). The 200 pA calibration bar is also valid for panels (A₂, A₃). (A₂, A₃) IPSCs during 10 and 100 Hz stimulation, respectively, from the same neuron as in panel (A₁). Similar to (A₁), the last IPSC during the 40-s-period is shown on the right (#400 and #4000, respectively). (B₁) Time course of IPSC peak amplitudes from two LSO neurons at stimulation frequencies ranging from 1–200 Hz (for color code, see inset). Peak values to the first 40 pulses (pulse #1–40) are plotted. (B₂) Like (B₁), but depicting the time course of IPSC peak amplitudes during the complete 40-s-periods. For each stimulation frequency, peak amplitudes were sampled at 1-s-intervals. Notice the stronger amount of STD than at 37°C , particularly at higher frequencies.

P11, because the latter displayed a statistically significant decline already at 50 Hz. Like at P11, mean peak IPSC_{30–40 s} amplitudes declined in a frequency-dependent manner in P19/ 37°C LSO neurons, but they remained above 25% of the control up to

100 Hz (Figures 7B₂, C, Table 1). Noticeably, this level was about 4-fold higher than at P11/ 37°C .

The moderate difference between P19/ 37°C and P11/ 37°C in STD behavior was also reflected by the failures. Interestingly, at virtually every stimulus frequency, both the percentage of neurons with failures and the failure rate were lower at P11 (Table 2). For example, at 100 Hz, 27% of the P11/ 37°C neurons displayed failures during the first 40 pulses (0.8% mean failure rate), whereas 40% of the P19/ 37°C neurons did so (3.5% mean failure rate). Thus, the performance of the MNTB-LSO connections shortly after hearing onset was surprisingly better in the millisecond range than that observed 1 week later. However, the opposite finding was achieved in the 40 s range, because P11 synapses displayed failure rates $>20\%$ at 50 Hz, whereas P19 synapses remained virtually failure-free up to 100 Hz (Table 2).

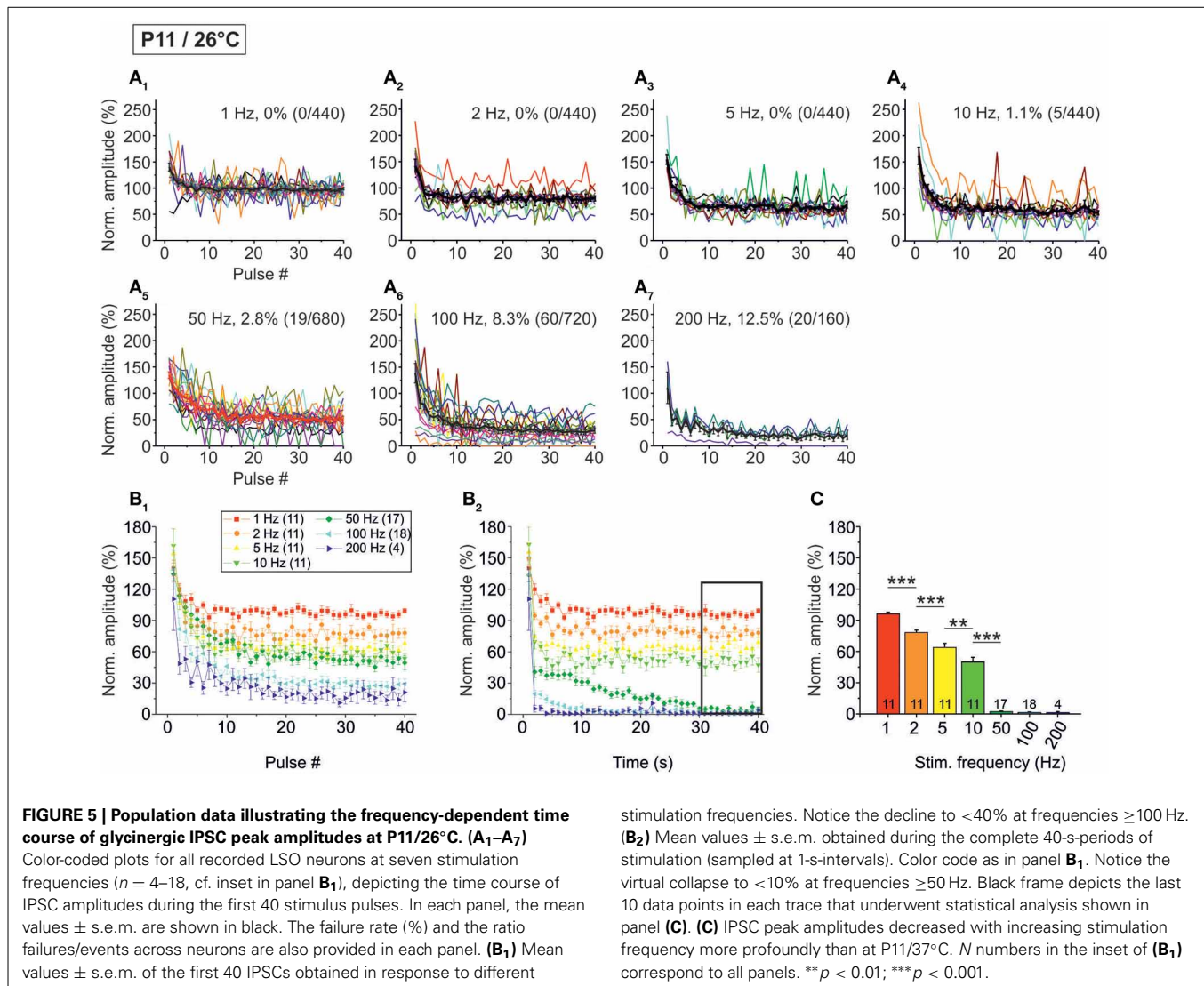
TEMPERATURE- AND AGE-DEPENDENCY OF IPSC KINETICS

IPSC kinetics at different temperatures and ages were determined from events obtained upon 1 Hz stimulation (Figure 8A; value for each neuron is the mean over 40 events). Concerning temperature dependency, the mean IPSC peak amplitude was 2-fold higher at 37°C than at 26°C (Figure 8B; P11/ 37°C : 303.8 ± 29.0 pA, $n = 31$; P11/ 26°C : 150.3 ± 16.9 pA, $n = 10$, $p = 4.8 \times 10^{-5}$). Noticeably, the absolute amplitudes should be treated carefully. First, they may have been reduced by the usage of kynurenic acid (Mok et al., 2009). Second, the driving force for inward-directed Cl⁻ flow may have been slightly artificial because of the chloride concentration of 2 mM in the whole-cell patch pipettes.

The time course of the IPSCs was significantly shorter at 37°C , as evidenced by a 2-fold shorter rise time (37°C : 0.4 ± 0.02 ms, $n = 29$; 26°C : 0.8 ± 0.1 ms, $n = 10$; $p = 6.9 \times 10^{-5}$) and a 1.5-fold shorter decay time (37°C : 2.2 ± 0.1 ms, $n = 30$; 26°C : 3.4 ± 0.3 ms, $n = 10$; $p = 0.002$). Analysis of age-dependency (P19/ 37°C vs. P11/ 37°C) revealed significant differences for all three parameters tested (Figure 8), such that P19 MNTB-LSO synapses displayed a 30% lower peak amplitude (194.4 ± 27.0 pA, $n = 13$; $p = 0.030$), a 25% shorter rise time (10–90%: 0.3 ± 0.02 ms, $n = 13$; $p = 6 \times 10^{-7}$) and a 2-fold shorter decay time ($\tau = 1.2 \pm 0.1$ ms, $n = 13$; $p = 5.2 \times 10^{-10}$).

TEMPERATURE-DEPENDENCY OF SYNAPTIC ATTENUATION AND RECOVERY

In a next series of experiments, we assessed the capacity of P11 LSO neurons to recover from synaptic attenuation. To do so, we again obtained an initial baseline for normalization (1 Hz, 40 s) and then stimulated uniformly with 50 Hz, now extending the stimulus train to 60 s (Figure 1B₂). Immediately thereafter, the stimulus frequency was reduced to 1 Hz, and IPSCs were recorded for another 60 s. In the following, we refer to these two 60-s epochs as challenge period and recovery period, respectively. Recordings were performed at 37°C ($n = 22$) and 26°C ($n = 17$). Exemplary results from a neuron at 26°C and another at 37°C are illustrated in Figures 9A₁, B₁, respectively, and the ensemble data are shown in Figures 9A₂, B₂. As expected, synapses displayed synaptic attenuation during the first 40 s as shown before (cf. Figures 3B₂, 5B₂). By the very end of the challenge period, peak IPSC amplitudes (IPSC_{60 s}) had completely collapsed to

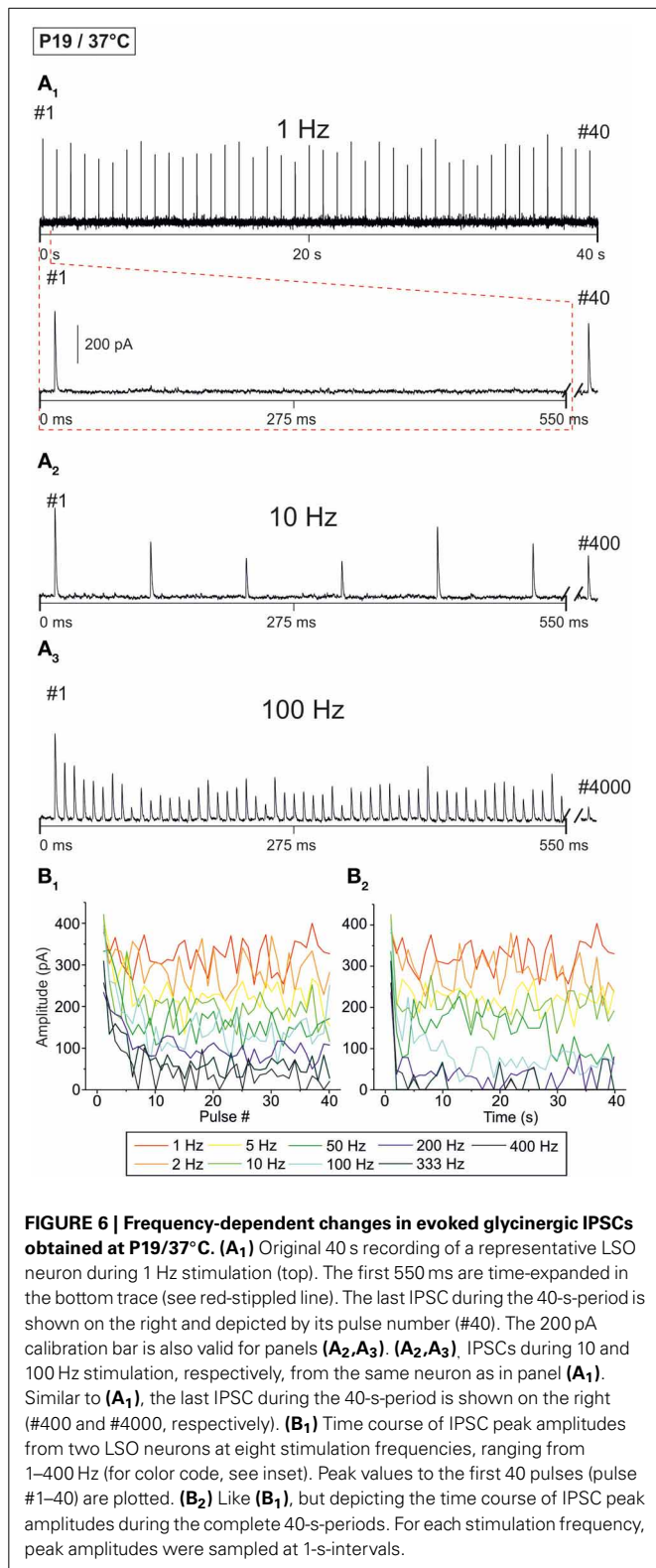


$0.0 \pm 0.0\%$ at 26°C , yet they remained at $20.6 \pm 3.3\%$ at 37°C (**Figures 9A₂,B₂**). The latter value did not differ significantly from that obtained after 40 s ($27.7 \pm 4.8\%$; $p = 0.226$), corroborating that 37°C responses are quite stable in the second-to-minute range. In contrast, IPSCs declined further between 40 and 60 s at 26°C (IPSC_{40s}: $2.9 \pm 1.4\%$; $p = 0.049$). Together, this demonstrates that glycinergic MNTB-LSO neurotransmission is sustained at a steady-state level in the minute range only at physiological temperature. The better performance in the minute range at 37°C was also evident in drastically higher peak amplitudes during the last 10 s of the challenge period: at 37°C , the mean IPSC_{50–60s} value was $23.3 \pm 3.5\%$, but it was almost 40-fold lower at 26°C ($0.6 \pm 0.2\%$; $p = 1 \times 10^{-6}$; **Figures 9C,D**).

During the recovery period, several failures occurred within the first 10 s (60–70 s), albeit considerably fewer at 37°C (26°C : 16.5%; 37°C : 1.4%, **Figures 9A₂,B₂, Table 4**). Thereafter (70–120 s), only two failures occurred in the 26°C group (0.2%, 2/850) and three failures in the 37°C group (0.3%, 3/1100), indicating that neurotransmission recovered within a few seconds,

regardless of temperature (**Figures 9A₂,B₂**). The course of recovery could be fitted with a mono-exponential function, resulting in τ -values of 9.1 ± 0.7 s at 26°C and 6.3 ± 0.9 s at 37°C (**Figures 9C,E**). Thus, the recovery at 26°C was almost 1.5-fold slower than at 37°C ($p = 0.016$). In comparison to recovery data obtained from IPSCs in other neuron types, the recovery of MNTB-LSO synapses was similarly fast (P14–14/32–33°C rat neocortex neurons: 4.3 s; (Galarreta and Hestrin, 1998); P10/room temp. rat spinal cord neurons: ca. 8 s; (Ingram et al., 2008); P13–15/31°C mouse cerebellar nucleus neurons: 10 s; (Telgkamp and Raman, 2002), ruling out that they are unusual or even unique in this respect.

At both temperatures, IPSC_{110–120s} peak amplitudes of the P11 MNTB-LSO connections were significantly higher than IPSC_{50–60s} amplitudes (**Table 3**; estimated recovery: 37°C : 3.6-fold; 26°C : 36.0-fold). IPSC_{110–120s} values amounted to $107.7 \pm 5.0\%$ of the control value at 26°C and thus were overshooting (cf. Dinkelacker et al., 2000). At 37°C , the corresponding value was significantly lower ($83.8 \pm 6.4\%$, $p = 0.007$; **Table 3; Figure 9D**).



SYNAPTIC ATTENUATION DURING VERY PROLONGED STIMULATION AT P11/37°C (10 TRIALS, 20 MIN, 50 Hz)

As the glycinergic neurotransmission recovered robustly after a 60-s-stimulus train (cf. Figure 9), we decided to challenge the

synapses even more with the aim to determine their limits. We extended the stimulation time and applied the 60 s/50 Hz challenge and 60 s/1 Hz recovery protocol for a total of ten times (Trial 1–10, Figure 1B₂), resulting in 30,600 pulses over a period of 20 min. The results from such “marathon experiments” are depicted in Figure 10. On average, the glycinergic MNTB-LSO neurotransmission was resistant to very prolonged stimulation, as evidenced by the fact that mean peak amplitudes did not decline below 15% (Figures 10A,B). Nevertheless, synaptic augmentation progressed, albeit only slightly, from trial to trial (Figure 10B, Table 3). For example, the mean IPSC_{50–60 s} in trial 10 was significantly lower than that in trial 1 ($18.3 \pm 3.6\%$ vs. $23.3 \pm 3.5\%$, $p = 0.020$). Likewise, the IPSC₁ amplitudes declined significantly, albeit only moderately, from trial 1 to trial 10 (Table 3). Similar effects were seen for IPSC₂, whereas IPSC₁₀ and IPSC_{1 s} did not decline during 20-min stimulation.

We also investigated the development of failures across trials during the challenge period. In a first step, we analyzed all IPSCs during the first 40 pulses. No failure was seen during trial 1, hardly any in trial 5 (0.4%), yet almost 10% in trial 10 (Table 4), indicative of some worsening with time. In a second step, we analyzed the failures during the last second of the challenge period (59–60 s). Whereas the percentage of neurons with failures increased only moderately (45.5% in trial 1, 57.1% in trial 5 and 10), the failure rate increased more than 2-fold (from 14.3% in trial 1 to 29.3% in trial 10; Table 4), again demonstrating some worsening performance with time.

SYNAPTIC ATTENUATION DURING VERY PROLONGED STIMULATION AT P11/26°C (10 TRIALS, 20 MIN, 50 Hz)

We next performed the “marathon experiments” at 26°C to assess temperature dependency (Figure 11). In contrast to 37°C, the mean IPSC₁ amplitude decreased drastically and highly significantly from trial 1–10, becoming more than 3-fold reduced (Table 3). Likewise, IPSC₂, IPSC₁₀, and IPSC_{1 s} decreased significantly with increasing trial number, and the effects were much more pronounced than at 37°C (Table 3). The time course of depression was similar across trials, resulting in almost completely collapsed amplitudes after about 35 s in each case. Mean IPSC_{50–60 s} peak amplitudes were <5% of the control, with a significant difference between trial 1 and 5 only (Table 3, Figure 11B), probably because amplitudes jittered considerably. This result was due to the almost complete collapse obvious already in trial 1.

Trial-to-trial development of the failures also displayed major differences between 26 and 37°C. During the first 40 pulses, the failure rate increased steadily from trial to trial, and much more rapidly than at 37°C. This was evidenced by a considerable increase from 14.3 to 22.3% between trial 1 and 5 at 26°C, yet a negligible increase from 0 to 0.4% at 37°C (Table 4). During the last second of the challenge period, however, there was no major difference in the failure rate between trials. Again, this can be explained by the fact that depression was already very robust in the first trial. Together, the failure rate was considerably higher than at 37°C.

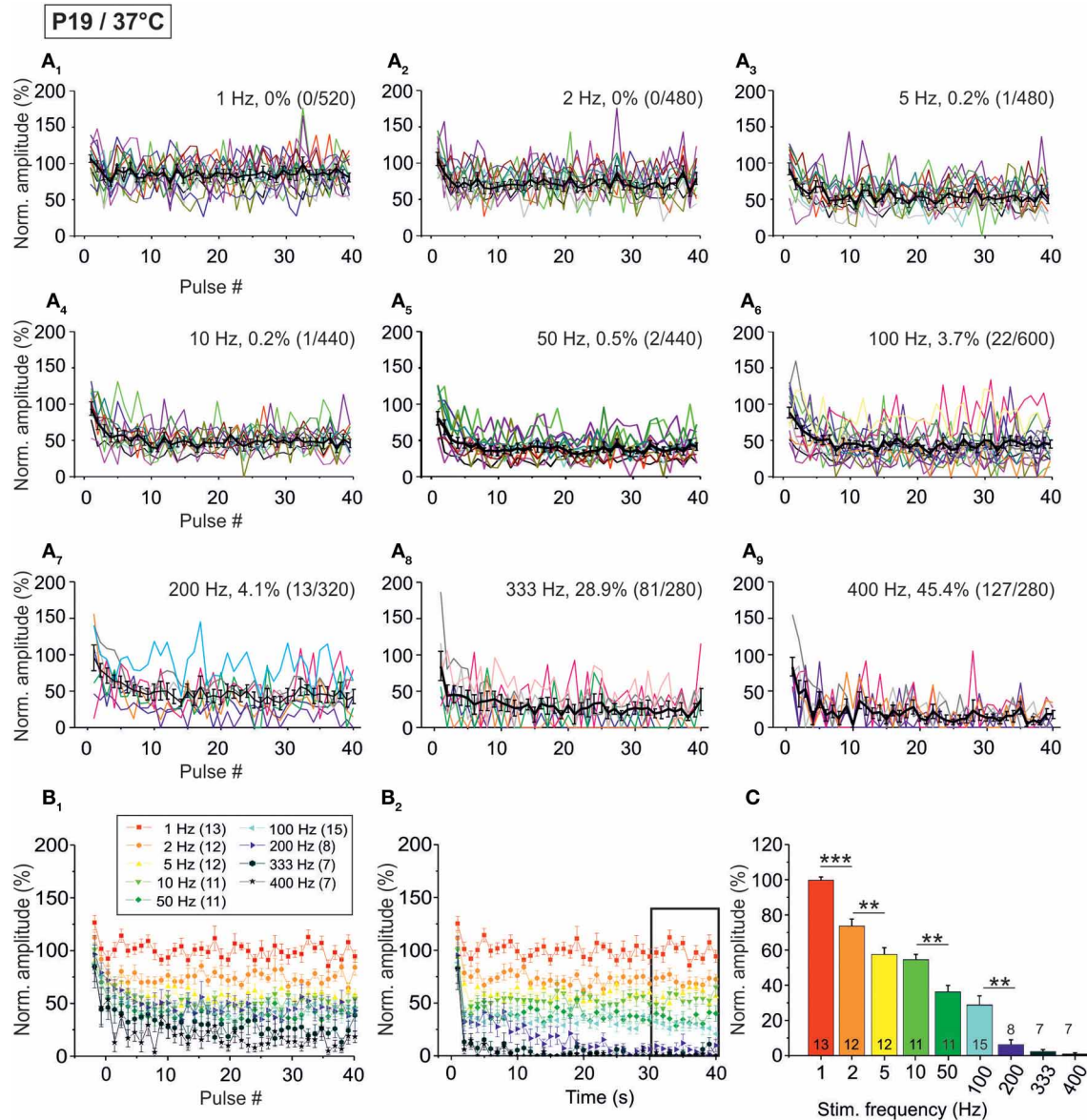


FIGURE 7 | Population data illustrating the frequency-dependent time course of glycinergic IPSC peak amplitudes at P19/37°C. (A₁–A₉),

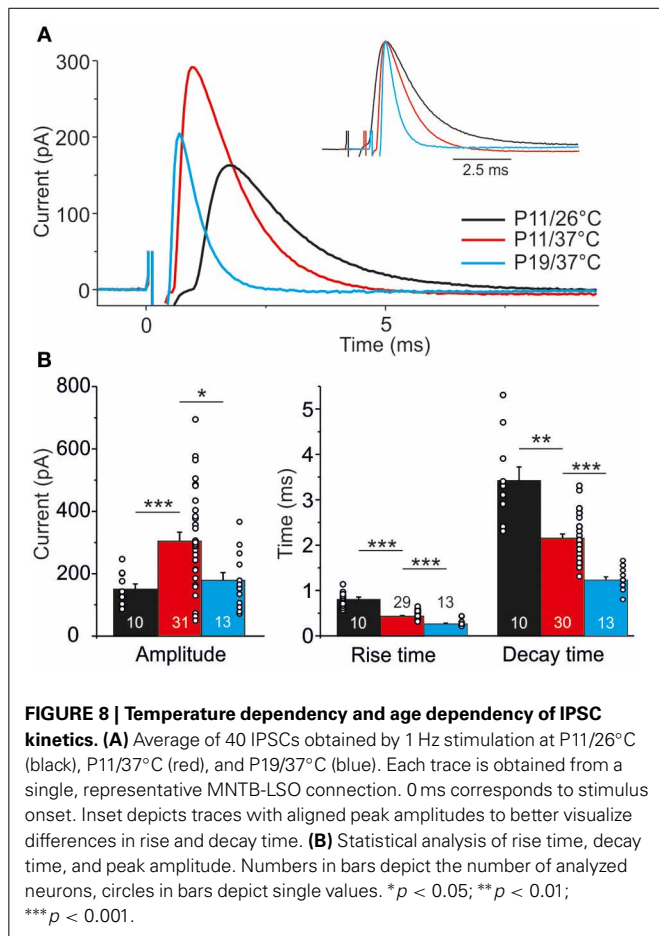
Color-coded plots for all recorded LSO neurons at nine stimulation frequencies ($n = 7$ –15, cf. inset in panel B₁), depicting the time course of IPSC amplitudes during the first 40 stimulus pulses. In each panel, the mean values \pm s.e.m. are shown in black. The failure rate (%) and the ratio failures/events across neurons are also provided in each panel. (B₁) Mean values \pm s.e.m. of the first 40 IPSCs obtained in response to different stimulation frequencies. Notice the decline to

<50% at frequencies ≥ 50 Hz. (B₂) Mean values \pm s.e.m. obtained during the complete 40-s-periods of stimulation (sampled at 1-s-intervals). Color code as in panel (B₁). Notice the gradual decline with frequency up to 200 Hz. Black frame depicts the last 10 data points in each trace that underwent statistical analysis shown in panel (C). (C) IPSC peak amplitudes decreased with increasing stimulation frequency, yet stayed at >30% of the control amplitude up to 100 Hz. N numbers in the inset of (B₁) correspond to all panels. ** $p < 0.01$; *** $p < 0.001$.

TEMPERATURE DEPENDENCY OF RECOVERY DURING VERY PROLONGED STIMULATION (10 TRIALS, 20 MIN, 50 Hz)

At both 37 and 26°C, the course of recovery from synaptic attenuation was quite variable across neurons, particularly in later trials (Figures 10A, 11A). As assessed by the $IPSC_{50-60s}/IPSC_{110-120s}$ ratios, peak amplitudes recuperated significantly in all trials and at both temperatures (Table 3), but at 37°C, the recovery courses were much more reproducible

(Figures 10B, 11B). At 37°C, mean $IPSC_{110-120s}$ amplitudes amounted to about 76.9–83.8% of the control value, with no significant differences between trial 1–5 and trial 1–10 (Figure 10B, Table 3). In contrast, mean $IPSC_{110-120s}$ amplitudes at 26°C became significantly reduced more than 2.5-fold (Figure 11B, Table 3, $107.7 \pm 5.0\%$ in trial 1, $43.9 \pm 5.5\%$ in trial 10). For a direct illustration of the temperature-dependent differences and for further quantification, we superimposed the curves obtained



at both temperatures during trial 1, 5, and 10 (Figure 12A). At the end of each challenge period, IPSC_{50–60s} values at 26°C were consistently lower than at 37°C (Figures 12A,B; $p = 1 \times 10^{-6}$, $p = 2 \times 10^{-4}$, $p = 1 \times 10^{-4}$ for trials 1, 5, 10). At the end of the recovery period, however, the situation was more diverse: at 37°C, IPSC_{110–120s} values were significantly lower than those obtained at 26°C in trial 1, yet they were higher in trial 10. No difference occurred in trial 5 (Figures 12A,C; $p = 0.007$, $p = 0.188$, $p = 0.005$ for trials 1, 5, 10).

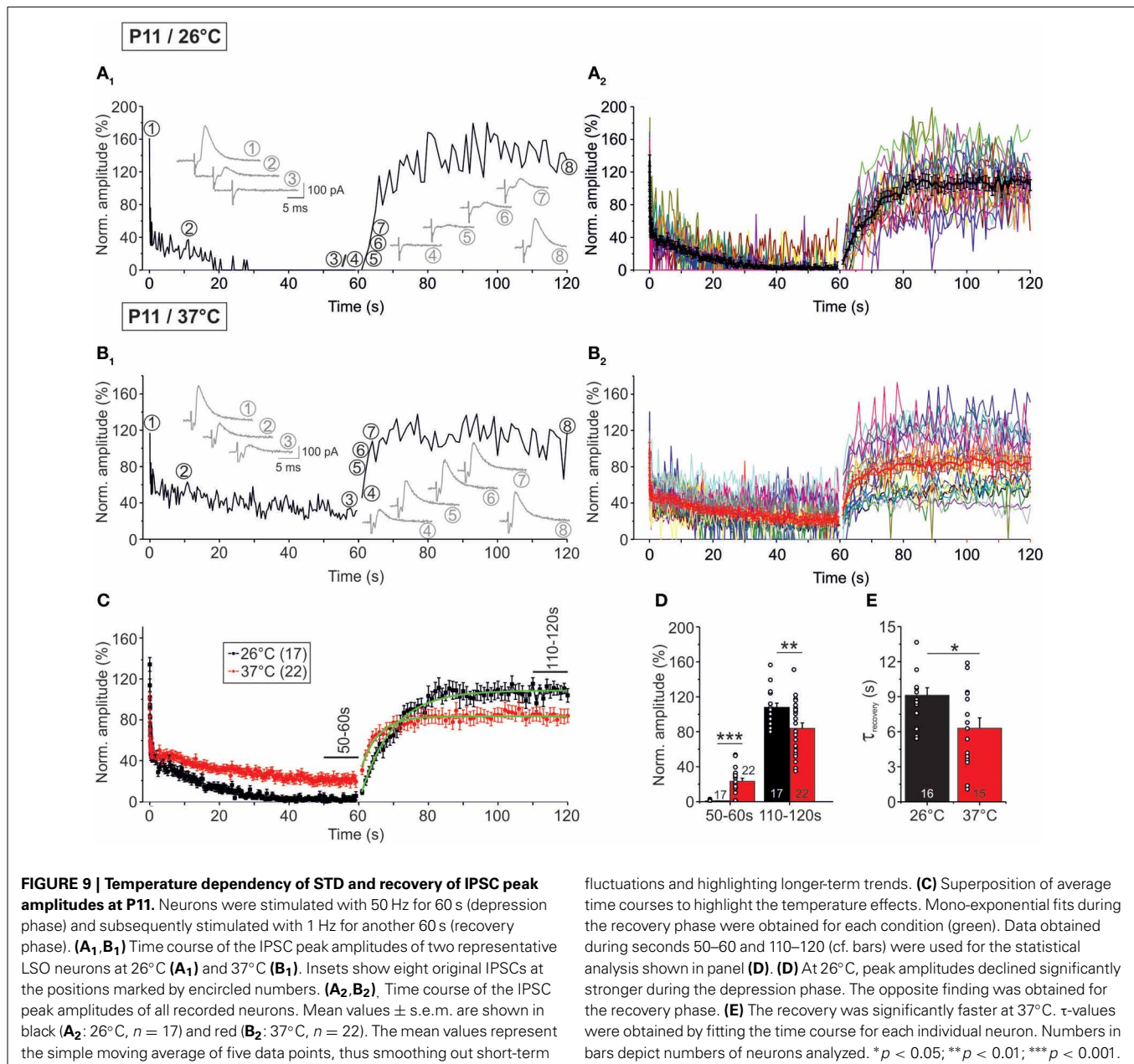
The temperature dependency of STD and amplitude recovery across trials was reflected by the time course of the failure rates. During the first 40 pulses at 37°C, failure rates of about 10% occurred in trial 10 only, whereas this level was reached already in trial 5 at 26°C (Table 4, Figure 12D). At the end of the challenge period (59–60s), the temperature effect on the failure rate was even more pronounced, because values at 26°C exceeded 60% in all trials (Table 4, Figure 12D). In contrast, the failure rate during 59–60s was drastically lower at 37°C (<30%), increasing moderately with trial number (Table 4, Figure 12D). Concerning the recovery at 37°C during the first 10s (60–70s), 9.1% of the neurons displayed failures in trial 1, whereas 14.3% did so both in trial 5 and trial 10, demonstrating a mild increase (Table 4). At 26°C, however, the percentage of neurons with failures was high already in trial 1 (52.9%) and remained high until the end (Table 4). Regarding

the 60–70s failure rate, the recovery of P11/37°C MNTB-LSO synapses was very good initially, yet it deteriorated from trial to trial and became 8.5-fold worse (trial 1: 1.4%; trial 10: 11.9%, Table 4, Figure 12E). In contrast, at 26°C the failure rate was much higher already from the beginning (trial 1: 16.5%) and remained at this high level during the “marathon experiment” (Table 4, Figure 12E). Thus, the performance at 37°C in the 20-min range was manifold superior to that at 26°C, but it also became less reliable with time. At the end of the recovery period (110–120s) in trial 1, the failure rate was negligible at both temperatures (Table 4, Figure 12E). By the time trial 10 was finished, however, it had increased considerably at both temperatures, with a similar rate of about 10% in both cohorts. Still, the percentage of neurons displaying failures at 26°C was almost twice as high as at 37°C (17.6 vs. 9.5%). Together, these data demonstrate a relatively minor trial-to-trial deterioration of the glycinergic MNTB-LSO transmission at physiological temperature, whereas at lower temperature, the performance becomes impaired quickly.

POSSIBLE CONTRIBUTION OF MNTB AXON CONDUCTION PROBLEMS TO IPSC FAILURES

In a final series of experiments, we addressed the question whether possible AP conduction problems (Bucher and Goiaillard, 2011) in axons of MNTB neurons may lead to the absence of neurotransmission and, therefore, to the absence of IPSCs. To do so, we compared our results obtained upon MNTB stimulation (orthodromic, synaptic) while recording from P11/37°C LSO neurons with those obtained via antidromic, non-synaptic stimulation of MNTB axons in the LSO while recording from MNTB neurons in the current-clamp mode. Orthodromic stimulation resulted in high-fidelity synaptic transmission during the first 40 pulses at stimulus frequencies from 1 to 200 Hz (Figures 13A₁,B₁). The great majority of neurons (6 of 8) displayed virtually no failures up to 100 Hz, but the fidelity declined to $98 \pm 2\%$ at 200 Hz and $84 \pm 0.13\%$ at 333 Hz (Figure 13C₁). During the last 40 pulses of the 40-s train, however, many more failures were apparent, and 100% fidelity was maintained only up to 10 Hz (Figures 13A₂–C₂). Above 10 Hz, the fidelity rate gradually declined to $83 \pm 12\%$ at 50 Hz and to $17 \pm 10\%$ at 333 Hz (Figure 13C₂). 90% fidelity (4 failures in 40 events) was computed at 280 Hz for the first 40 pulses and at 28 Hz for the last 40 pulses.

In the antidromic stimulation experiments, the pattern of successful responses (APs) and failures was quite similar to that obtained via orthodromic stimulation (Figures 13D–F). The performance declined with increasing stimulus frequency, such that APs occurred in response to the first 40 pulses in $93 \pm 5\%$ of cases at 100 Hz and $83 \pm 11\%$ at 200 Hz (Figure 13F₁). No failure occurred at frequencies ≤ 50 Hz. During the last 40 pulses, the performance was worse, the respective values being $45 \pm 13\%$ at 100 Hz and $6 \pm 4\%$ at 200 Hz (Figure 13F₂). Ninety percent fidelity occurred at 160 Hz during the first 40 pulses and at 55 Hz during the last 40 pulses. Thus, axons of P11/37°C MNTB neurons can conduct APs absolutely reliably up to 50 Hz, even upon very prolonged stimulation. Collectively, the results from orthodromic and antidromic stimulation show



that some fidelity decrease in synaptic transmission of the MNTB-LSO connection can be attributed to impaired AP conduction properties of MNTB neurons, rather than to deficits of the synaptic transmission machinery. However, the observed STD behavior is unlikely due to AP conduction problems and is rather a presynaptic effect (as further addressed in the Discussion).

DISCUSSION

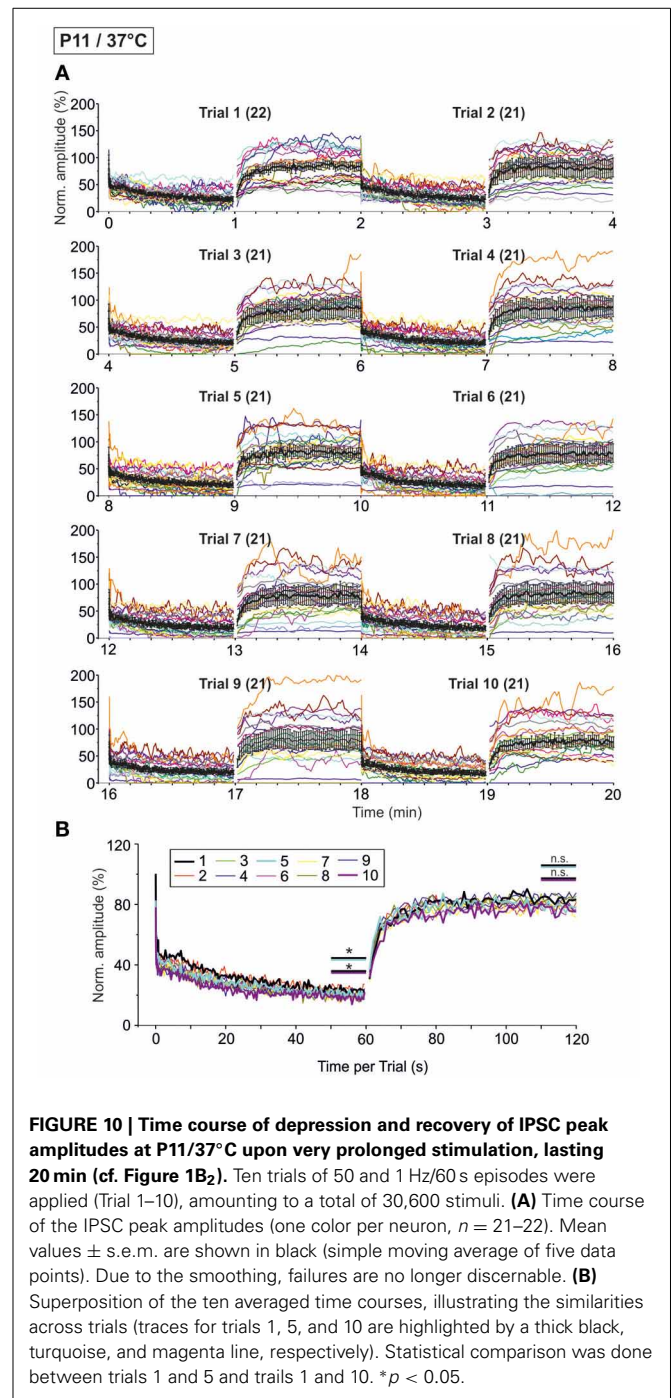
Mature LSO neurons receive powerful inhibitory, glycinergic input from MNTB neurons, which are able to respond reliably to high frequency stimulation supplied via the excitatory calyx of Held, up to 800 Hz for brief trains lasting ca. 20 ms (Taschenberger and von Gersdorff, 2000; Mc Laughlin et al.,

2008). Our results provide evidence that the subsequent glycinergic MNTB-LSO connections are less astounding in this time range, as they sustain faithful synaptic transmission merely to considerably lower frequencies (ca. 100 Hz at P11/37°C, cf. **Figure 3**). Although featuring robust STD and synaptic attenuation, the P11/37°C connections are nevertheless continuously functional in the 10 s-to-1 min range and, if recovery periods are introduced, neurotransmission is reliably sustained for at least 20 min upon 50 Hz stimulation. The performance crucially depends on temperature, as at 26°C, faithful neurotransmission falls close at >10 Hz, and collapses almost completely during prolonged stimulation with 50 Hz. Our data also demonstrate some moderate maturational changes from P11 to P19. The unusually short glycinergic IPSC decay time likely reflects specifically fast

Table 3 | IPSC peak amplitudes during challenge and recovery periods upon prolonged stimulation (20 min, 50 Hz).

		P11/37°C					P11/26°C				
		Challenge		Recovery			Challenge		Recovery		
	<i>n</i>	IPSC ₁	IPSC ₂	IPSC ₁₀	IPSC _{1s}	IPSC _{50-60s}	<i>n</i>	IPSC _{110-120s}	IPSC _{50-60s} /IPSC _{110-120s} [P]	Estimated recovery	
Trial 1	22	100.2 ± 5.1	83.9 ± 4.6	49.4 ± 3.2	45.6 ± 3.4	23.3 ± 3.5	Trial 1	83.8 ± 6.4	0.277 ± 0.033 [0.00004]	3.6-fold	
Trial 5	21	82.7 ± 7.4	70.0 ± 5.7	41.8 ± 3.4	42.5 ± 4.4	20.7 ± 3.8	Trial 5	81.4 ± 6.4	0.235 ± 0.031 [0.00006]	4.3-fold	
Trial 10	21	78.1 ± 10.5	69.8 ± 8.5	41.1 ± 5.2	36.7 ± 4.7	18.3 ± 3.6	Trial 10	76.9 ± 9.4	0.227 ± 0.035 [0.0002]	4.4-fold	
<i>P</i> : Trial 1 vs. Trial 5		0.014	0.013	0.158	0.581	0.048	<i>P</i> : Trial 1 vs. Trial 5	0.261			
<i>P</i> : Trial 1 vs. Trial 10		0.029	0.096	0.204	0.196	0.020	<i>P</i> : Trial 1 vs. Trial 10	0.385			
Trial 1	17	133.5 ± 6.7	113.7 ± 6.6	68.7 ± 8.1	43.8 ± 4.8	0.6 ± 0.2	Trial 1	107.7 ± 5.0	0.028 ± 0.017 [0.0003]	36.0-fold	
Trial 5	17	59.5 ± 8.1	59.2 ± 6.4	45.9 ± 6.3	33.8 ± 5.2	4.1 ± 1.0	Trial 5	68.4 ± 7.2	0.050 ± 0.021 [0.0004]	20.0-fold	
Trial 10	17	38.4 ± 5.6	37.6 ± 5.1	28.2 ± 3.6	25.3 ± 5.2	1.6 ± 0.5	Trial 10	43.9 ± 5.5	0.037 ± 0.011 [0.0004]	27.0-fold	
<i>P</i> : Trial 1 vs. Trial 5		7E-06	3E-06	0.005	0.132	0.003	<i>P</i> : Trial 1 vs. Trial 5	3E-06			
<i>P</i> : Trial 1 vs. Trial 10		2E-08	4E-10	4E-05	0.003	0.069	<i>P</i> : Trial 1 vs. Trial 10	3E-09			

n, number of neurons. A Wilcoxon-signed rank test was used to account for obvious non-normality of the data, as, e.g., the mean IPSC_{50-60s} equaled 0 in some neurons (complete collapse of responses). Due to the same reason, the ratio IPSC_{30-60s}/IPSC_{110-120s} was determined, instead of the inverse ratio. The estimated recovery is the inverse ratio (e.g., 20-fold, if IPSC_{30-60s}/IPSC_{110-120s} = 0.05). Moreover, as some neurons featured mean IPSC values of 0 in the challenge and the recovery phase, they were excluded from the IPSC_{50-60s}/IPSC_{110-120s} analysis. Consequently, *n* = 22, 21, 18 at 37°C and 17, 16, 16 at 26°C in the Wilcoxon-signed rank test.



deactivation kinetics of GlyRs in LSO neurons, and thus rapid channel closure, which optimizes the integration of interaural intensity differences. On the other hand, the relatively normal recovery course from STD rules out a specific, ultrafast replenishment machinery in glycinergic MNTB-LSO synapses (Cho et al., 2011). STD in glycinergic synapses is much less studied than in GABAergic synapses, and analyses are surprisingly limited to the auditory system, where they are only recent and rudimentary (Couchman et al., 2010; Kuo and Trussell, 2011). The present

Table 4 | Failure rate analysis during challenge and recovery periods upon prolonged stimulation (20 min, 50 Hz).

P11/37°C					
Challenge			Recovery		
First 40 pulses	Neurons with failures (%) [ratio]	Failure rate (%) [failures/events]	60–70 s	Neurons with failures (%) [ratio]	Failure rate (%) [failures/events]
Trial 1	0 [0/22]	0 [0/880]	Trial 1	9.1 [2/22]	1.4 [3/220]
Trial 5	9.5 [2/21]	0.4 [3/840]	Trial 5	14.3 [3/21]	3.3 [7/210]
Trial 10	23.8 [5/21]	9.9 [83/840]	Trial 10	14.3 [3/21]	11.9 [25/210]
59–60 s	Neurons with failures (%) [ratio]	Failure rate (%) [failures/events]	110–120 s	Neurons with failures (%) [ratio]	Failure rate (%) [failures/events]
Trial 1	45.5 [10/22]	14.3 [157/1100]	Trial 1	4.5 [1/22]	0.5 [1/220]
Trial 5	57.1 [12/21]	22.3 [234/1050]	Trial 5	0 [0/21]	0 [0/210]
Trial 10	57.1 [12/21]	29.3 [308/1050]	Trial 10	9.5 [2/21]	9.5 [20/210]
P11/26°C					
Challenge			Recovery		
First 40 pulses	Neurons with failures (%) [ratio]	Failure rate (%) [failures/events]	60–70 s	Neurons with failures (%) [ratio]	Failure rate (%) [failures/events]
Trial 1	11.8 [2/17]	2.8 [19/680]	Trial 1	52.9 [9/17]	16.5 [28/170]
Trial 5	17.6 [3/17]	10.4 [71/680]	Trial 5	29.4 [5/17]	14.1 [24/170]
Trial 10	35.3 [6/16]	14.0 [95/680]	Trial 10	47.1 [8/17]	20.0 [34/170]
59–60 s	Neurons with failures (%)	Failure rate (%) [failures/events]	110–120 s	Neurons with failures (%) [ratio]	Failure rate (%) [failures/events]
Trial 1	100 [17/17]	70.7 [601/850]	Trial 1	0 [0/17]	0 [0/170]
Trial 5	100 [17/17]	67.5 [574/850]	Trial 5	11.8 [2/17]	9.4 [16/170]
Trial 10	100 [17/17]	81.1 [689/850]	Trial 10	17.6 [3/17]	11.8 [20/170]

study provides the most extensive analysis of glycinergic short-term plasticity so far, and it also provides a fresh look into neurotransmission within a prolonged time window. In contrast to most studies, yet similar to two previous reports (Galarreta and Hestrin, 1998; Klyachko and Stevens, 2006), our analysis comprised normalization of the peak amplitude of IPSC₁ and all subsequent IPSCs to a control value (average from 40 IPSCs obtained at 1 Hz stimulus frequency prior to high frequency stimulation; **Figures 1B₁, B₂**). Under these conditions, mean peak amplitudes of IPSC₁, which was always evoked after a 3-min pause, exceeded 110% at every stimulus frequency when recordings were performed at 26°C (**Table 1, Figures 5B₁, B₂**). We propose that this initial overshoot may be due to disturbed and imprecise regulation of docking and/or priming processes, resulting in an increased number of fusion-competent vesicles after long periods of synaptic silence (cf. Hermann et al., 2007; Klug, 2011; Klug et al., 2012), for very similar treatises on the lack of chronic background activity on short-term plasticity). As such overshooting IPSCs were rare at 37°C, the disturbed regulation appears to be mainly a temperature artifact. It may also explain the overshooting recovery course in trial 1 at 26°C (**Table 3, Figures 9C, D**). Furthermore, our results add a general

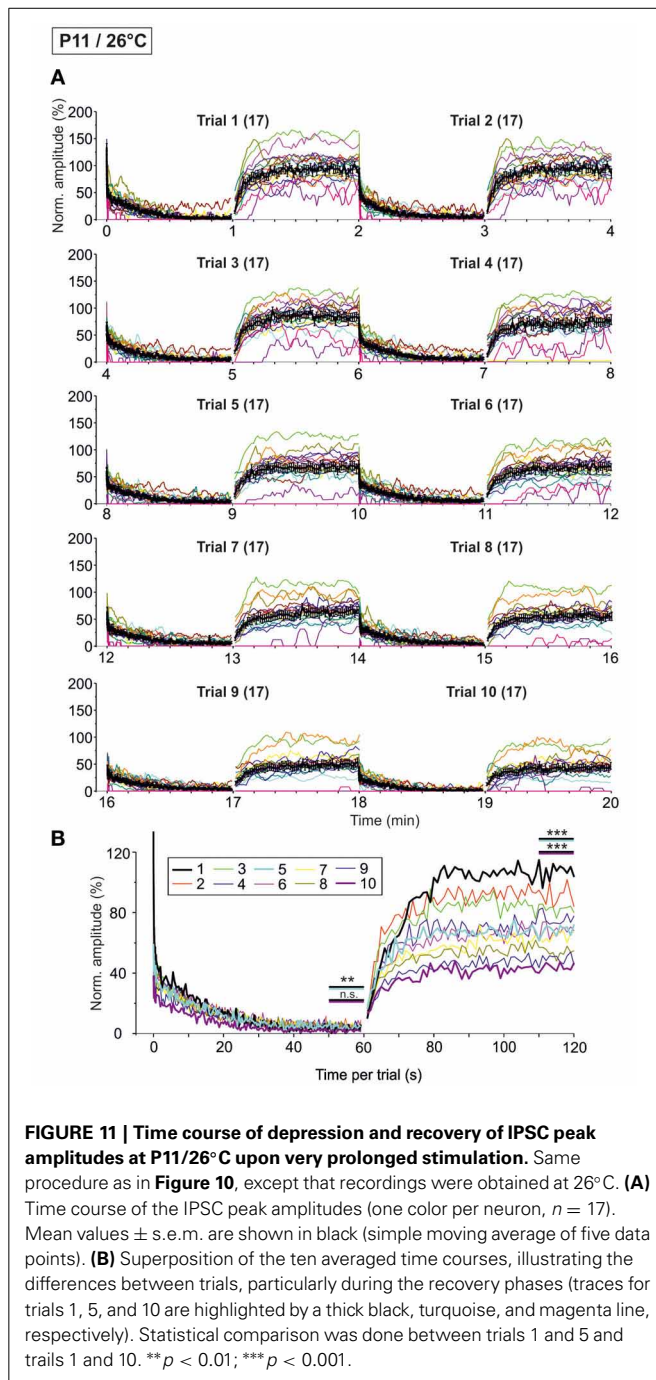
caveat to room temperature studies, because they overestimate the amplitude of the first event and, consequently, the amount of STD.

IPSC KINETICS

The decay times (P11/37°C: 2.2 ms; P19/37°C: 1.2 ms) were similar to estimated time constants described previously for rodent LSO principal neurons (mouse: 1.3 ms at P21–45/34°C, (Wu and Kelly, 1995); 4.6 ms at P9–19/25°C; (Sterenborg et al., 2010); gerbil: 2.6 ms at P17–23/31–32°C, (Sanes, 1990), yet it was considerably slower than the IPSC decay time constants reported for several other CNS neurons, e.g., P60/33–34°C mouse somatosensory cortex neurons (5.7 ms; Bragina et al., 2008), P7/30–32°C rat spinal cord motoneurons (7.2–17.0 ms; Sadlaoud et al., 2010), P28–35/29°C mouse amygdala neurons (24.1–41.4 ms; Song et al., 2013), P3/35°C chick nucleus laminaris neurons (10.4–54.8 ms; Tang and Lu, 2012), and P4/30°C chick vestibular nuclei neurons (10.5 ms; Shao et al., 2012).

CHARACTERISTICS OF STD

In virtually all of our recordings, IPSC peak amplitudes declined rapidly within the first 10 events, such that the IPSC₁₀ amplitudes



reached a fraction of the control value at stimulus frequencies ≥ 5 Hz, regardless of age and temperature (cf. **Figures 3B₁, 5B₁, 7B₁**). Our results further show a prominent frequency dependency. When comparing the amount of STD observed in the present study with data obtained from various synapse types within and outside the auditory system, STD in the glycinergic MNTB-LSO connections is neither particularly high nor low, but tends to be on the low side (**Table 5**, cf. values for 100 Hz stimulus frequency). We found no indication for short-term facilitation, consistent with the idea that STD is key to maintaining temporal

precision (Kuba et al., 2002; Cook et al., 2003). The absence of short-term facilitation at P11 and P19 in the MNTB-LSO synapses makes a developmental regulation of short-term plasticity unlikely within this time period, namely depression in younger and facilitation in mature synapses, as described for glutamatergic EPSPs in the rat neocortex between P14 and P18 (Reyes and Sakmann, 1999) and for GABAergic IPSCs in the gerbil auditory cortex after hearing onset (Takesian et al., 2010). Interestingly, preliminary results obtained from P30 MNTB-LSO connections also revealed no short-term facilitation, but STD, consistent with findings from mature endbulb of Held synapses (Wang and Manis, 2008).

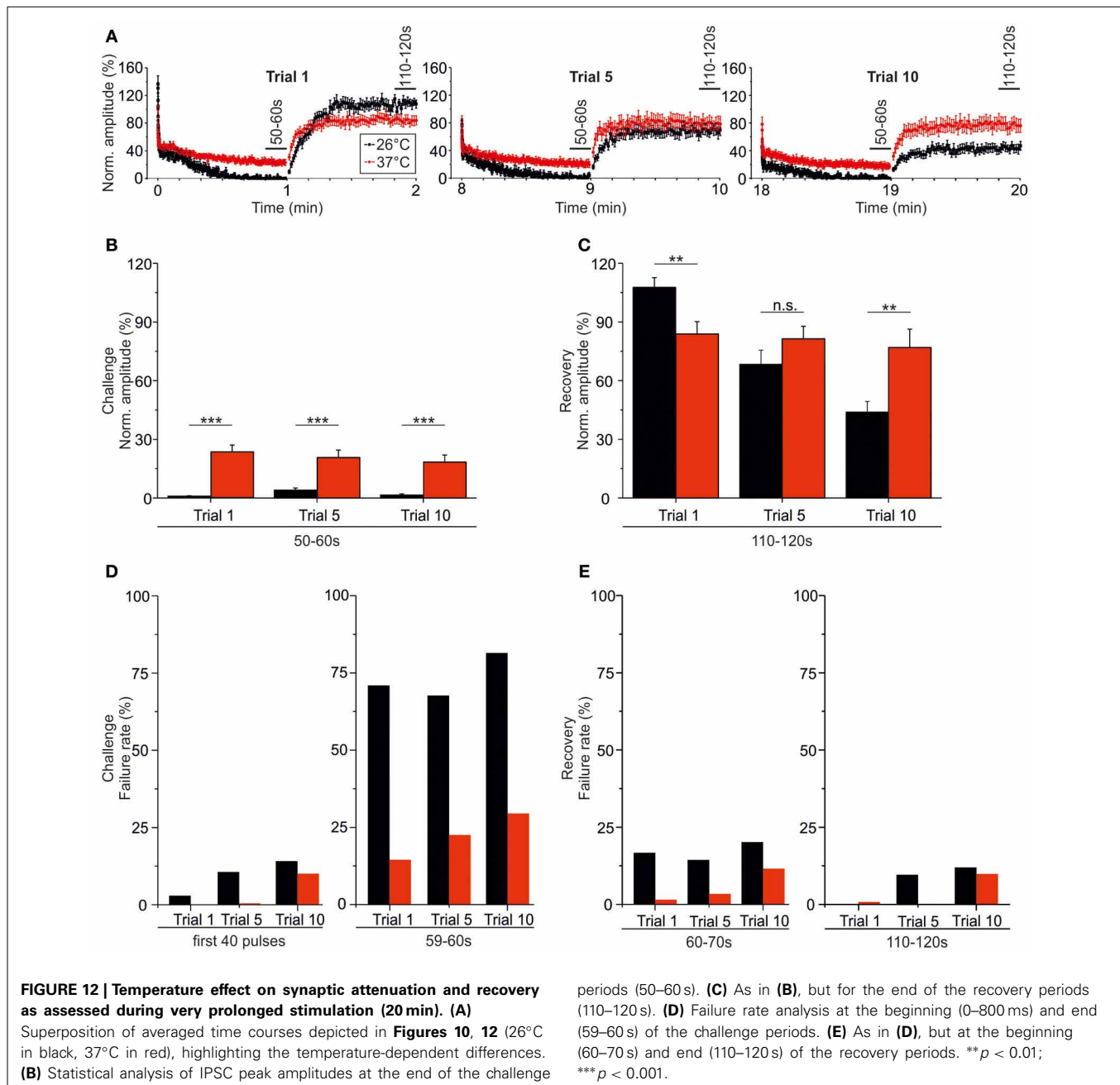
PLATEAU PHASE DURING PROLONGED STIMULATION

An interesting observation in the course of STD was a plateau phase, which was centered at 3–4 s and lasted several seconds. This plateau phase was particularly evident at P11/37°C during 50 Hz stimulation (**Figure 9C**). A similar phenomenon, named delayed response enhancement, has been described in glutamatergic hippocampal synapses, where it depends on presynaptic synapsins I and II, is temperature-dependent, and most prominent in adults “marathon experiments.” The underlying mechanism of this plateau phase in the glycinergic MNTB-LSO connections needs to be characterized in future studies.

RELIABILITY DURING VERY PROLONGED STIMULATION

The present study is quite novel in that the vast majority of studies so far have assessed synaptic depression with very few tetanic pulses (ca. 20), whereas we have stimulated over a period of 60 s and in 10 trials, resulting in 30,600 stimuli total (marathon experiments). We did so because the IPSC peak amplitudes had not reached a steady state after 20 pulses. Rather, they further declined considerably, e.g., reaching values of $<30\%$ after 40 s at 50Hz/P11/37°C (cf. **Table 1**, **Figure 3B₂**). These results are consistent with the rare results described elsewhere for such IPSCs, namely in the hippocampus (Klyachko and Stevens, 2006). EPSCs in this intermediate range have been analyzed more extensively, for example in the calyx-MNTB synapse (deLange et al., 2003), primary hippocampal neurons (Sara et al., 2002), autaptic hippocampal neurons (Lambert et al., 2010), and the neuromuscular junction (Richards et al., 2003). Together the results, like ours, show that STD does not reach a plateau level during the first 1–2 s of tetanic stimulation. In our case, steady state was not reached until about 30 s into the experiment.

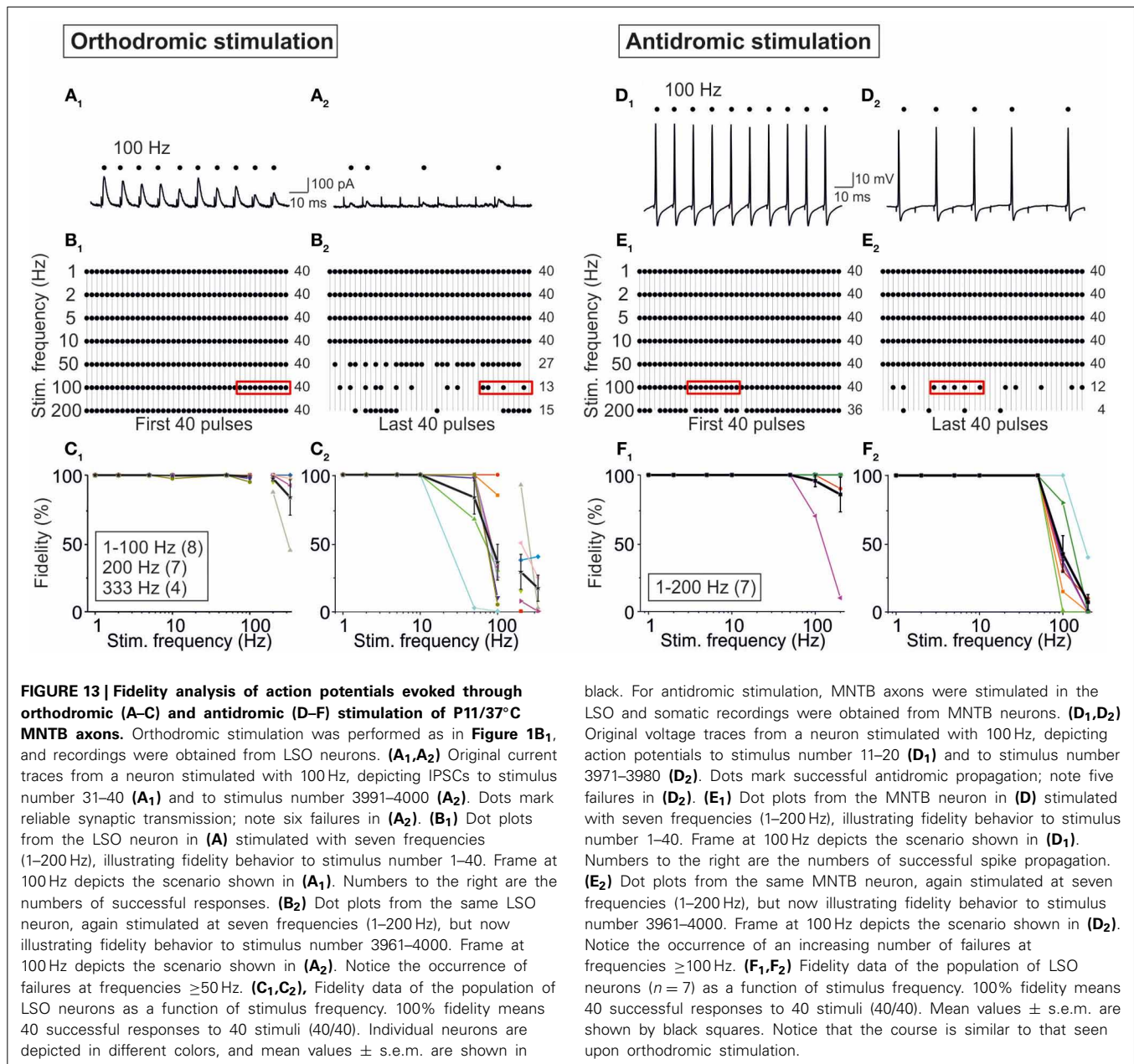
Glycinergic IPSC peak amplitudes of the MNTB-LSO connection were not depressed below 20%, and the failure rate was remarkably low, even when stimulation lasted ≥ 1 min (P11/37°C/50 Hz; cf. **Figure 10B**, **Table 4**). As our stimulus paradigm included a 1-min-long recovery period between subsequent 1-min challenge epochs, we cannot rule out that IPSC peak amplitudes will diminish further when the stimulus train is extended beyond 1 min. Preliminary results (Bakker and Friauf, unpublished) indeed demonstrate a further decline when stimulation lasts 10 min, yet the transmission stays functional, with mean peak amplitudes amounting to about 15% during the last minute.



PARTICIPATION OF GABA_B RECEPTORS?

As shown in gerbils, LSO neurons release GABA during spiking activity which acts as a retrograde transmitter at presynaptic GABA_B receptors, leading to an adjustment of the synaptic strength (Magnusson et al., 2008) and rendering the system more dynamic (Grothe and Koch, 2011). Such a scenario can be ruled out in our experiments which were done under voltage-clamp conditions, thus preventing spike generation. Moreover, in current-clamp conditions, the glycinergic MNTB-LSO neurotransmission would have been hyperpolarizing because of the chloride concentrations used in the bath and

pipette solutions. Therefore, we conclude that retrograde signaling via presynaptic GABA_B receptors was not confounded by our pharmacological blockade of these receptors with CGP55845. Still, GABA may have been co-released together with glycine from the axon terminals of MNTB neurons (Kotak et al., 1998; Nabekura et al., 2004; Wojcik et al., 2006) and, thereby, GABA_B receptors may have been affected. However, control experiments in the absence of CGP55845 (not shown) did not reveal any effect on the time course of synaptic depression and recovery. Thus, we exclude a considerable role of GABA_B receptor signaling from our experiments.



PRE- OR POSTSYNAPTIC MECHANISM OF DEPRESSION?

STD can be caused by depletion of transmitter release (von Gersdorff and Matthews, 1997). Likewise, postsynaptic receptors can be desensitized (Jones and Westbrook, 1996; Overstreet et al., 2000) or saturated (Kirischuk et al., 2002) by repetitive exposure to neurotransmitter. However, in contrast to GABA_A receptors (Jones and Westbrook, 1995), GlyRs do not desensitize heavily, i.e., they do not enter long-lived closed states in the prolonged presence of glycine (Akaike and Kaneda, 1989; Lewis et al., 1991; Melnick and Baev, 1993; Harty and Manis, 1996; Breiting et al., 2004; Mørkve and Hartveit, 2009). Therefore, we conclude that the observed STD is a presynaptic phenomenon. STD is often ascribed to depletion of the readily releasable vesicle pool (Rizzoli and Betz, 2005).

Inactivation of presynaptic Ca²⁺ channels (Forsythe et al., 1998; Xu and Wu, 2005; Hennig et al., 2008; Mochida et al., 2008) or the refractoriness of release sites during repetitive activation (Dittman et al., 2000) are also feasible (see González-Inchauspe et al., 2007, for counterarguments). In contrast, feedback activation of presynaptic autoreceptors, as shown for GABA, glutamate, and adenosine (Takahashi et al., 1998; Zucker and Regehr, 2002), appears to be unlikely, because high-affinity metabotropic GlyRs are unknown. Quite to the contrary, activation of presynaptic ionotropic GlyRs opens presynaptic Cl⁻ channels, which in turn depolarizes the terminal, resulting in opening of voltage-operated Ca²⁺ channels, elevated presynaptic [Ca²⁺]_i, and, ultimately, enhanced neurotransmitter release (Turecek and Trussell, 2001; Zucker and Regehr, 2002). Our

Table 5 | Comparison of STD in several neuronal systems.

	Synapse type	System	Species	Age	Temperature (°C)	Stimulus frequency (Hz)	Amount of STD (%)	References
1	Glycinergic IPSCs	MNTB-LSO	Mouse	P11 P19 P11	37 37 26	50, 100	51, 50 48, 70 68, 49	Present study
2	Glycinergic IPSCs	MNTB-LSO	Mouse	P11–15	23–25	20	42	Giugovaz-Tropper et al., 2011
3	IPSCs	MNTB-LSO	Gerbil, Mouse	P10–18	32	100	73	Walcher et al., 2011
4	GABAergic IPSPs	IC-MGB	Rat	P8 P16 P27	35	5, 10, 50	77, 77, 93 37, 49, 91 51, 62, 89	Venkataraman and Bartlett, 2013
5	EPSCs	Calyx-MNTB	Mouse	P12–15	20–22	100, 200, 300	50, 65, 85	Wang and Kaczmarek, 1998
6	EPSCs	Calyx-MNTB	Rat	P8–11	21–25	0.5, 10, 100	33, 75, 92	von Gersdorff et al., 1997
7	EPSCs	Calyx-MNTB	Rat	P5–7 P12–14	35	10, 100, 300	85, 95, 95 55, 70, 80	Taschenberger and von Gersdorff, 2000
8	EPSCs	Calyx-MNTB	Rat	P6–10	22–25	20	75	deLange et al., 2003
9	EPSCs	Calyx-MNTB	Mouse	P11–16	22–25	100	70	Oleskevich et al., 2004
10	EPSCs	Endbulb-VCN	Mouse	P11–16	22–25	100	>80	Oleskevich and Walmsley, 2002; Oleskevich et al., 2004
11	EPSCs	Endbulb-VCN	Mouse	P15–21	34	100	>67	Yang and Xu-Friedman, 2008
12	EPSCs	Endbulb-VCN	Mouse	P15–21	34	100	35	Wang and Manis, 2008
13	EPSCs and IPSCs	MSO	Gerbil	P60–100	35	100	70	Couchman et al., 2010
14	EPSCs	Ncl. magnocellularis	Chick	E16–17	31–35	200	85	Zhang and Trussell, 1994
15	EPSCs	Ncl. laminaris	Chick	E18–21	37	100	75	Cook et al., 2003
16	GABAergic IPSCs	Ncl. laminaris	Chick	E17–P3	35	50, 100, 200	40, 75, 85	Tang and Lu, 2012
17	GABAergic IPSCs	Auditory cortex	Gerbil	P8–11 P17–22 P25–30	32	25	87 27 5	Takesian et al., 2010
18	GABAergic IPSCs	Neocortex	Rat	P14–17	32–33	20	60	Galarreta and Hestrin, 1998
19	GABAergic IPSCs	Visual cortex	Rat	P13–19	32–35	20, 50	45, 55	Varela et al., 1999
20	GABAergic IPSCs	Hypothalamus	Rat	P21–27	32.5	10, 20, 50	51, 59, 72	Baimoukhametova et al., 2004
21	GABAergic IPSCs	Hippocampus	Rat	P20–24	34	50	64	Hefft et al., 2002
22	GABAergic IPSCs	Hippocampus	Rat	P14–25	33.5	40	40	Klyachko and Stevens, 2006
22	GABAergic IPSCs	Purkinje cells-Cerebellar nuclei	Mouse	P13–15	31	50	50	Telgkamp and Raman, 2002
24	GABAergic IPSCs	Amygdala	Mouse	P28–35	29	20	66–84	Song et al., 2013
25	GABAergic IPSCs	Spinal cord	Rat	P3–21	Room temp.	10	40	Ingram et al., 2008
26	GABAergic IPSCs	Visual cortex	Rat	P35	Room temp.	30	60	Jiang et al., 2010
27	GABAergic IPSCs	Somatosensory cortex	Mouse	P15–23	32	20	63–87	Ma et al., 2012

Publications 1–17 have analyzed STD in inhibitory and excitatory synapses in the auditory system, publications 18–27 in inhibitory, GABAergic synapses outside the auditory system. For the sake of clarity, the Table does not list any data on short-term facilitation. In each case, the amount of STD is given by: $100 \times (1 - PSC_{10}/PSC_1)$. In order to allow for a direct comparison between our data and those published, we have recalculated our data listed in **Table 1** accordingly. Abbreviations: IC, inferior colliculus; LSO, lateral superior olive; MGB, medial geniculate body; MNTB, medial nucleus of the trapezoid body; MSO, medial superior olive; VCN, ventral cochlear nucleus.

results of increased STD at lower temperature are also in line with a presynaptic effect, because physiological temperatures accelerate vesicle recruitment and reduce STD (Kushmerick et al., 2006). Finally, we can rule out a collapse of the chloride driving force in the LSO neurons during repetitive stimulation (Ehrlich et al., 1999), and thus a postsynaptic effect, because we performed our experiments in the whole-cell mode, thereby clamping E_{Cl} to -112 mV and generating a constant driving force.

Our results from antidromic stimulation experiments imply that AP conduction failures, which occurred only at stimulus frequencies ≥ 100 Hz, do not at all contribute to impaired

transmission at frequencies ≤ 50 Hz. Rather, the presynaptic release machinery cannot faithfully follow such frequencies, resulting in failures. Furthermore, as the fidelity of AP conduction at 100 Hz was 45% (**Figure 13F₂**), and as about eight MNTB neurons converge onto a single LSO neuron (Noh et al., 2010; Hirtz et al., 2012), the probability that all of these eight neurons simultaneously display a conduction failure calculates to 1% ($55\%^8$). This low value does not explain the 64% failures in IPSCs (cf. **Figure 13C₂**). Only at 200 Hz, AP conduction failures appear to contribute to IPSC failures, because the probability of an AP conduction failure in all eight converging MNTB neurons ($94\%^8 = 61\%$) comes close to the observed IPSC failure rate of

71%. Finally, also the course of recovery cannot be explained by spike failures.

In sum, although glycinergic MNTB-LSO connections undergo STD and synaptic attenuation, they can sustain high frequency transmission at hearing onset over long periods (minutes) and thousands of stimuli if stimulus frequency does not exceed 50 Hz. They also recover robustly ($\tau = 6.3$ s). At P11, connections appear to function quite reliably, yet sustained transmission at 100 Hz is reached only by P19. If the physiological temperature is reduced by 11°C, the performance worsens drastically, in that 10 Hz is now the upper frequency for reliable transmission. Depletion of transmitter release is the most likely cause of the depression behavior. It is important to assess the impact of glycine recycling in replenishing the transmitter pool. One aspect is neuronal and glial re-uptake from the synaptic cleft, which is mediated by glycine transporters 1 and 2, respectively. The role of these transporters may be addressed in pharmacological (Jeong et al., 2010; Jiménez et al., 2011) and genetic knock-out experiments (Gomez et al., 2003a,b), employing the same battery of stimuli as used in the present study.

AUTHOR CONTRIBUTIONS

Eckhard Friauf, Florian Kramer, and Désirée Griesemer designed the study; Florian Kramer, Dennis Bakker, Sina Brill, and Erik Frotscher performed the experiments; Eckhard Friauf, Désirée Griesemer, Jürgen Franke, and Florian Kramer analyzed data and wrote the paper.

ACKNOWLEDGMENTS

This work was supported by the Deutsche Forschungsgemeinschaft (DFG Grant FR 1784/17-1 to Eckhard Friauf) and the DFG Research Training Group “Molecular, physiological and pharmacological analysis of cellular membrane transport” (GRK 845, Florian Kramer and Eckhard Friauf). Further support was provided by the Center for Mathematical and Computational Modeling, Kaiserslautern. We thank Jennifer Winkelhoff for excellent technical support and Dr. Marco Rust, Dr. Jonathan Stephan, and Alex Fischer for valuable comments on an earlier version of the manuscript.

REFERENCES

- Akaike, N., and Kaneda, M. (1989). Glycine-gated chloride current in acutely isolated rat hypothalamic neurons. *J. Neurophysiol.* 62, 1400–1409.
- Awatramani, G. B., Turecek, R., and Trussell, L. O. (2005). Staggered development of GABAergic and glycinergic transmission in the MNTB. *J. Neurophysiol.* 93, 819–828. doi: 10.1152/jn.00798.2004
- Baimoukhametova, D. V., Hewitt, S. A., Sank, C. A., and Bains, J. S. (2004). Dopamine modulates use-dependent plasticity of inhibitory synapses. *J. Neurosci.* 24, 5162–5171. doi: 10.1523/JNEUROSCI.4979-03.2004
- Balakrishnan, V., Becker, M., Löhre, S., Nothwang, H. G., Güresir, E., and Friauf, E. (2003). Expression and function of chloride transporters during development of inhibitory neurotransmission in the auditory brainstem. *J. Neurosci.* 23, 4134–4145.
- Barry, P. H. (1994). JPCalc, a software package for calculating liquid junction potential corrections in patch-clamp, intracellular, epithelial and bilayer measurements and for correcting junction potential measurements. *J. Neurosci. Methods* 51, 107–116. doi: 10.1016/0165-0270(94)90031-0
- Bender, K. J., and Trussell, L. O. (2011). Synaptic plasticity in inhibitory neurons of the auditory brainstem. *Neuropharmacology* 60, 774–779. doi: 10.1016/j.neuropharm.2010.12.021
- Borst, J. G. G., and Soria van Hoeve, J. (2012). The calyx of Held synapse: from model synapse to auditory relay. *Annu. Rev. Physiol.* 74, 199–224. doi: 10.1146/annurev-physiol-020911-153236
- Bragina, L., Marchionni, I., Omrani, A., Cozzi, A., Pellegrini-Giampietro, D. E., Cherubini, E., et al. (2008). GAT-1 regulates both tonic and phasic GABA(A) receptor-mediated inhibition in the cerebral cortex. *J. Neurochem.* 105, 1781–1793. doi: 10.1111/j.1471-4159.2008.05273.x
- Breitinger, H. G., Lanig, H., Vohwinkel, C., Grever, C., Breitinger, U., Clark, T., et al. (2004). Molecular dynamics simulation links conformation of a pore-flanking region to hyperekplexia-related dysfunction of the inhibitory glycine receptor. *Chem. Biol.* 11, 1339–1350. doi: 10.1016/j.chembiol.2004.07.008
- Bucher, D., and Goaillard, J. M. (2011). Beyond faithful conduction: short-term dynamics, neuromodulation, and long-term regulation of spike propagation in the axon. *Prog. Neurobiol.* 94, 307–346. doi: 10.1016/j.pneurobio.2011.06.001
- Cho, S., Li, G. L., and von Gersdorff, H. (2011). Recovery from short-term depression and facilitation is ultrafast and Ca²⁺ dependent at auditory hair cell synapses. *J. Neurosci.* 31, 5682–5692. doi: 10.1523/JNEUROSCI.5453-10.2011
- Cook, D. L., Schwandt, P. C., Grande, L. A., and Spain, W. J. (2003). Synaptic depression in the localization of sound. *Nature* 421, 66–70. doi: 10.1038/nature01248
- Couchman, K., Grothe, B., and Felmy, F. (2010). Medial superior olivary neurons receive surprisingly few excitatory and inhibitory inputs with balanced strength and short-term dynamics. *J. Neurosci.* 30, 17111–17121. doi: 10.1523/JNEUROSCI.1760-10.2010
- deLange, R. P. J., deRoos, A. D. G., and Borst, J. G. G. (2003). Two modes of vesicle recycling in the rat calyx of Held. *J. Neurosci.* 23, 10164–10173.
- Dinkelacker, V., Voets, T., Neher, E., and Moser, T. (2000). The readily releasable pool of vesicles in chromaffin cells is replenished in a temperature-dependent manner and transiently overfills at 37°C. *J. Neurosci.* 20, 8377–8383.
- Dittman, J. S., Kreitzer, A. C., and Regehr, W. G. (2000). Interplay between facilitation, depression, and residual calcium at three presynaptic terminals. *J. Neurosci.* 20, 1374–1385.
- Ehret, G. (1976). Development of absolute auditory thresholds in the house mouse. *J. Am. Audiol. Soc.* 1, 179–184.
- Ehret, G., and Romand, R. (1992). Development of tone response thresholds, latencies and tuning in the mouse inferior colliculus. *Dev. Brain Res.* 67, 317–326. doi: 10.1016/0165-3806(92)90233-M
- Ehrlich, I., Löhre, S., and Friauf, E. (1999). Shift from depolarizing to hyperpolarizing glycine action in rat auditory neurons is due to age-dependent Cl⁻ regulation. *J. Physiol. (Lond.)* 520, 121–137. doi: 10.1111/j.1469-7793.1999.00121.x
- Forsythe, I. D., Tsujimoto, T., BarnesDavies, M., Cuttle, M. F., and Takahashi, T. (1998). Inactivation of presynaptic calcium current contributes to synaptic depression at a fast central synapse. *Neuron* 20, 797–807. doi: 10.1016/S0896-6273(00)81017-X
- Galarreta, M., and Hestrin, S. (1998). Frequency-dependent synaptic depression and the balance of excitation and inhibition in the neocortex. *Nat. Neurosci.* 1, 587–594. doi: 10.1038/2882
- Giugovaz-Tropper, B., González-Inchauspe, C., Di Guimi, M. N., Urbano, F. J., Forsythe, I. D., and Uchitel, O. D. (2011). P/Q-type calcium channel ablation in a mice glycinergic synapse mediated by multiple types of Ca(2+) channels alters transmitter release and short term plasticity. *Neuroscience* 192, 219–230. doi: 10.1016/j.neuroscience.2011.06.021
- Gomez, J., Hülsmann, S., Ohno, K., Eulenburg, V., Szöke, K., Richter, D., et al. (2003a). Inactivation of the glycine transporter 1 gene discloses vital role of glial glycine uptake in glycinergic inhibition. *Neuron* 40, 785–796. doi: 10.1016/S0896-6273(03)00672-X
- Gomez, J., Ohno, K., Hülsmann, S., Armsen, W., Eulenburg, V., Richter, D. W., et al. (2003b). Deletion of the mouse glycine transporter 2 results in a hyperekplexia phenotype and postnatal lethality. *Neuron* 40, 797–806. doi: 10.1016/S0896-6273(03)00673-1
- González-Inchauspe, C., Forsythe, I. D., and Uchitel, O. D. (2007). Changes in synaptic transmission properties due to the expression of N-type calcium channels at the calyx of Held synapse of mice lacking P/Q-type calcium channels. *J. Physiol.* 584, 835–851. doi: 10.1113/jphysiol.2007.139683
- Grothe, B., and Koch, U. (2011). Dynamics of binaural processing in the mammalian sound localization pathway - The role of GABA(B) receptors. *Hear. Res.* 279, 43–50. doi: 10.1016/j.heares.2011.03.013
- Harty, T. P., and Manis, P. B. (1996). Glycine-evoked currents in acutely dissociated neurons of the guinea pig ventral cochlear nucleus. *J. Neurophysiol.* 75, 2300–2311.

- Hefft, S., Kraushaar, U., Geiger, J. R., and Jonas, P. (2002). Presynaptic short-term depression is maintained during regulation of transmitter release at a GABAergic synapse in rat hippocampus. *J. Physiol.* 539, 201–208. doi: 10.1113/jphysiol.2001.013455
- Hennig, M. H., Postlethwaite, M., Forsythe, I. D., and Graham, B. P. (2008). Interactions between multiple sources of short-term plasticity during evoked and spontaneous activity at the rat calyx of Held. *J. Physiol.* 586, 3129–3146. doi: 10.1113/jphysiol.2008.152124
- Hermann, J., Pecka, M., von Gersdorff, H., Grothe, B., and Klug, A. (2007). Synaptic transmission at the calyx of Held under *in vivo*-like activity levels. *J. Neurophysiol.* 98, 807–820. doi: 10.1152/jn.00355.2007
- Hirtz, J. J., Braun, N., Griesemer, D., Hanned, C., Janz, K., Löhrike, S., et al. (2012). Synaptic refinement of an inhibitory topographic map in the auditory brainstem requires functional Cav1.3 calcium channels. *J. Neurosci.* 32, 14602–14616. doi: 10.1523/JNEUROSCI.0765-12.2012
- Humberto, S., Garcia-Oscos, F., Lu, D., and Atzori, M. (2011). Dynamic modulation of short term synaptic plasticity in the auditory cortex: the role of norepinephrine. *Hear. Res.* 271, 26–36. doi: 10.1016/j.heares.2010.08.014
- Ingram, R. A., Fitzgerald, M., and Bacceti, M. L. (2008). Developmental changes in the fidelity and short-term plasticity of GABAergic synapses in the neonatal rat dorsal horn. *J. Neurophysiol.* 99, 3144–3150. doi: 10.1152/jn.01342.2007
- Jeong, H. J., Vandenberg, R. J., and Vaughan, C. W. (2010). N-arachidonyl-glycine modulates synaptic transmission in superficial dorsal horn. *Br. J. Pharmacol.* 161, 925–934. doi: 10.1111/j.1476-5381.2010.0935.x
- Jiang, B., Huang, S., Pasquale, R., Millman, D., Song, L., Lee, H. K., et al. (2010). The maturation of GABAergic transmission in visual cortex requires endocannabinoid-mediated LTD of inhibitory inputs during a critical period. *Neuron* 66, 248–259. doi: 10.1016/j.neuron.2010.03.021
- Jiménez, E., Zafra, F., Pérez-Sen, R., Delicado, E. G., Miras-Portugal, M. T., Aragón, C., et al. (2011). P2Y purinergic regulation of the glycine neurotransmitter transporters. *J. Biol. Chem.* 286, 10712–10724. doi: 10.1074/jbc.M110.167056
- Jones, M. V., and Westbrook, G. L. (1995). Desensitized states prolong GABA_A channel responses to brief agonist pulses. *Neuron* 15, 181–191. doi: 10.1016/0896-6273(95)90075-6
- Jones, M. V., and Westbrook, G. L. (1996). The impact of receptor desensitization on fast synaptic transmission. *Trends Neurosci.* 19, 96–101. doi: 10.1016/S0166-2236(96)80037-3
- Kandler, K. (2004). Activity-dependent organization of inhibitory circuits: lessons from the auditory system. *Curr. Opin. Neurobiol.* 14, 96–104. doi: 10.1016/j.conb.2004.01.017
- Kim, G., and Kandler, K. (2003). Elimination and strengthening of glycinergic/GABAergic connections during tonotopic map formation. *Nat. Neurosci.* 6, 282–290. doi: 10.1038/nn1015
- Kirischuk, S., Clements, J. D., and Grantyn, R. (2002). Presynaptic and postsynaptic mechanisms underlie paired pulse depression at single GABAergic boutons in rat collicular cultures. *J. Physiol.* 543, 99–116. doi: 10.1113/jphysiol.2002.021576
- Klug, A. (2011). Short-term synaptic plasticity in the auditory brain stem by using *in-vivo*-like stimulation parameters. *Hear. Res.* 279, 51–59. doi: 10.1016/j.heares.2011.05.011
- Klug, A., Borst, J. G., Carlson, B. A., Kopp-Scheinflug, C., Klyachko, V. A., and Xu-Friedman, M. A. (2012). How do short-term changes at synapses fine-tune information processing? *J. Neurosci.* 32, 14058–14063. doi: 10.1523/JNEUROSCI.3348-12.2012
- Klyachko, V. A., and Stevens, C. F. (2006). Excitatory and feed-forward inhibitory hippocampal synapses work synergistically as an adaptive filter of natural spike trains. *PLoS Biol.* 4:e207. doi: 10.1371/journal.pbio.0040207
- Kotak, V. C., Korada, S., Schwartz, I. R., and Sanes, D. H. (1998). A developmental shift from GABAergic to glycinergic transmission in the central auditory system. *J. Neurosci.* 18, 4646–4655.
- Kuba, H., Koyano, K., and Ohmori, H. (2002). Synaptic depression improves coincidence detection in the nucleus laminaris in brainstem slices of the chick embryo. *Eur. J. Neurosci.* 15, 984–990. doi: 10.1046/j.1460-9568.2002.01933.x
- Kuo, S. P., and Trussell, L. O. (2011). Spontaneous spiking and synaptic depression underlie noradrenergic control of feed-forward inhibition. *Neuron* 71, 306–318. doi: 10.1016/j.neuron.2011.05.039
- Kushmerick, C., Renden, R., and von Gersdorff, H. (2006). Physiological temperatures reduce the rate of vesicle pool depletion and short-term depression via an acceleration of vesicle recruitment. *J. Neurosci.* 26, 1366–1377. doi: 10.1523/JNEUROSCI.3889-05.2006
- Lalor, E. C., Power, A. J., Reilly, R. B., and Foxe, J. J. (2009). Resolving precise temporal processing properties of the auditory system using continuous stimuli. *J. Neurophysiol.* 102, 349–359. doi: 10.1152/jn.90896.2008
- Lambert, T. J., Storm, D. R., and Sullivan, J. M. (2010). MicroRNA132 modulates short-term synaptic plasticity but not basal release probability in hippocampal neurons. *PLoS ONE* 29:e15182. doi: 10.1371/journal.pone.0015182
- Lewis, C. A., Ahmed, Z., and Faber, D. S. (1991). A characterization of glycinergic receptors present in cultured rat medullary neurons. *J. Neurophysiol.* 66, 1291–1303.
- Lieberman, M. C. (1978). Auditory nerve response from cats raised in a low-noise chamber. *J. Acoust. Soc. Am.* 63, 442–455. doi: 10.1121/1.381736
- Ma, Y. Y., Hu, H., and Agmon, A. (2012). Short-term plasticity of unitary inhibitory-to-inhibitory synapses depends on the presynaptic interneuron subtype. *J. Neurosci.* 32, 983–988. doi: 10.1523/JNEUROSCI.5007-11.2012
- MacLeod, K. M. (2011). Short-term synaptic plasticity and intensity coding. *Hear. Res.* 279, 13–21. doi: 10.1016/j.heares.2011.03.001
- Magnusson, A. K., Park, T. J., Pecka, M., Grothe, B., and Koch, U. (2008). Retrograde GABA signaling adjusts sound localization by balancing excitation and inhibition in the brainstem. *Neuron* 59, 125–137. doi: 10.1016/j.neuron.2008.05.011
- Mc Laughlin, M., van der Heijden, M., and Joris, P. X. (2008). How secure is *in vivo* synaptic transmission at the calyx of Held? *J. Neurosci.* 28, 10206–10219. doi: 10.1523/JNEUROSCI.2735-08.2008
- Melnick, I. V., and Baev, K. V. (1993). Glycine conductance changes in chick spinal cord neurons developing in culture. *Neuroscience* 52, 347–360. doi: 10.1016/0306-4522(93)90162-9
- Mikaelian, D., and Ruben, R. J. (1965). Development of hearing in the normal CBA-J mouse. *Acta Oto-Laryngol.* 59, 451–461. doi: 10.3109/00016486509124579
- Mochida, S., Few, A. P., Scheuer, T., and Catterall, W. A. (2008). Regulation of presynaptic Ca_v2.1 channels by Ca²⁺ sensor proteins mediates short-term synaptic plasticity. *Neuron* 57, 210–216. doi: 10.1016/j.neuron.2007.11.036
- Mok, S. M. H., Fricker, A. C., Weil, A., and Kew, J. N. C. (2009). Electrophysiological characterisation of the actions of kynurenic acid at ligand-gated ion channels. *Neuropharmacology* 57, 242–249. doi: 10.1016/j.neuropharm.2009.06.003
- Mørkve, S. H., and Hartveit, E. (2009). Properties of glycine receptors underlying synaptic currents in presynaptic axon terminals of rod bipolar cells in the rat retina. *J. Physiol. (Lond.)* 587, 3813–3830. doi: 10.1113/jphysiol.2009.173583
- Nabekura, J., Katsurabayashi, S., Kakazu, Y., Shibata, S., Matsubara, A., Jinno, S., et al. (2004). Developmental switch from GABA to glycine release in single-central synaptic terminals. *Nat. Neurosci.* 7, 17–23. doi: 10.1038/nn1170
- Noh, J., Seal, R. P., Garver, J. A., Edwards, R. H., and Kandler, K. (2010). Glutamate co-release at GABA/glycinergic synapses is crucial for the refinement of an inhibitory map. *Nat. Neurosci.* 13, 232–238. doi: 10.1038/nn.2478
- Oleskevich, S., and Walmsley, B. (2002). Synaptic transmission in the auditory brainstem of normal and congenitally deaf mice. *J. Physiol.* 540, 447–455. doi: 10.1113/jphysiol.2001.013821
- Oleskevich, S., Youssofian, M., and Walmsley, B. (2004). Presynaptic plasticity at two giant auditory synapses in normal and deaf mice. *J. Physiol.* 560, 709–719. doi: 10.1113/jphysiol.2004.066662
- Overstreet, L. S., Jones, M. V., and Westbrook, G. L. (2000). Slow desensitization regulates the availability of synaptic GABA(A) receptors. *J. Neurosci.* 20, 7914–7921.
- Regehr, W. G. (2012). Short-term presynaptic plasticity. *Cold Spring Harb. Perspect. Biol.* 4:a005702. doi: 10.1101/cshperspect.a005702
- Reyes, A., and Sakmann, B. (1999). Developmental switch in the short-term modification of unitary EPSPs evoked in layer 2/3 and layer 5 pyramidal neurons of rat neocortex. *J. Neurosci.* 19, 3827–3835.
- Richards, D. A., Guatimosim, C., Rizzoli, S. O., and Betz, W. J. (2003). Synaptic vesicle pools at the frog neuromuscular junction. *Neuron* 39, 529–541. doi: 10.1016/S0896-6273(03)00405-7
- Rizzoli, S. O., and Betz, W. J. (2005). Synaptic vesicle pools. *Nat. Rev. Neurosci.* 6, 57–69. doi: 10.1038/nrn1583
- Sadlaoui, K., Tazerart, S., Brocard, C., Jean-Xavier, C., Partialier, P., Brocard, F., et al. (2010). Differential plasticity of the GABAergic and glycinergic synaptic transmission to rat lumbar motoneurons after spinal cord injury. *J. Neurosci.* 30, 3358–3369. doi: 10.1523/JNEUROSCI.6310-09.2010

- Sanes, D. H. (1990). An *in vitro* analysis of sound localization mechanisms in the gerbil lateral superior olive. *J. Neurosci.* 10, 3494–3506.
- Sanes, D. H., and Friauf, E. (2000). Development and influence of inhibition in the lateral superior olivary nucleus. *Hear. Res.* 147, 46–58. doi: 10.1016/S0378-5955(00)00119-2
- Sara, Y., Mozhayeva, M. G., Liu, X., and Kavalali, E. T. (2002). Fast vesicle recycling supports neurotransmission during sustained stimulation at hippocampal synapses. *J. Neurosci.* 22, 1608–1617.
- Shao, M., Hirsch, J. C., and Peusner, K. D. (2012). Plasticity of spontaneous excitatory and inhibitory synaptic activity in morphologically defined vestibular nuclei neurons during early vestibular compensation. *J. Neurophysiol.* 107, 29–41. doi: 10.1152/jn.00406.2011
- Song, C., Xu, X. B., He, Y., Liu, Z. P., Wang, M., Zhang, X., et al. (2013). Stuttering interneurons generate fast and robust inhibition onto projection neurons with low capacity of short term modulation in mouse lateral amygdala. *PLoS ONE* 8:e60154. doi: 10.1371/journal.pone.0060154
- Sonntag, M., Englitz, B., Kopp-Scheinpflug, C., and Rübsamen, R. (2009). Early postnatal development of spontaneous and acoustically evoked discharge activity of principal cells of the medial nucleus of the trapezoid body: an *in vivo* study in mice. *J. Neurosci.* 29, 9510–9520. doi: 10.1523/JNEUROSCI.1377-09.2009
- Sonntag, M., Englitz, B., Typlt, M., and Rübsamen, R. (2011). The calyx of Held develops adult-like dynamics and reliability by hearing onset in the mouse *in vivo*. *J. Neurosci.* 31, 6699–6709. doi: 10.1523/JNEUROSCI.0575-11.2011
- Sterenborg, J. C., Pilati, N., Sheridan, C. J., Uchitel, O. D., Forsythe, I. D., and Barnes-Davies, M. (2010). Lateral olivocochlear (LOC) neurons of the mouse LSO receive excitatory and inhibitory synaptic inputs with slower kinetics than LSO principal neurons. *Hear. Res.* 270, 119–126. doi: 10.1016/j.heares.2010.08.013
- Takahashi, T., Kajikawa, Y., and Tsujimoto, T. (1998). G-protein-coupled modulation of presynaptic calcium currents and transmitter release by a GABA_B receptor. *J. Neurosci.* 18, 3138–3146.
- Takesian, A. E., Kotak, V. C., and Sanes, D. H. (2010). Presynaptic GABA_B receptors regulate experience-dependent development of inhibitory short-term plasticity. *J. Neurosci.* 30, 2716–2727. doi: 10.1523/JNEUROSCI.3903-09.2010
- Tang, Z. Q., and Lu, Y. (2012). Two GABA_A responses with distinct kinetics in a sound localization circuit. *J. Physiol.* 590, 3787–3805. doi: 10.1113/jphysiol.2012.230136
- Taschenberger, H., Leao, R. M., Rowland, K. C., Spirou, G. A., and von Gersdorff, H. (2002). Optimizing synaptic architecture and efficiency for high-frequency transmission. *Neuron* 36, 1127–1143. doi: 10.1016/S0896-6273(02)01137-6
- Taschenberger, H., and von Gersdorff, H. (2000). Fine-tuning an auditory synapse for speed and fidelity: developmental changes in presynaptic waveform, EPSC kinetics, and synaptic plasticity. *J. Neurosci.* 20, 9162–9173.
- Telgkamp, P., and Raman, I. M. (2002). Depression of inhibitory synaptic transmission between Purkinje cells and neurons of the cerebellar nuclei. *J. Neurosci.* 22, 8447–8457.
- Temchin, A. N., Rich, N. C., and Ruggero, M. A. (2008). Threshold tuning curves of chinchilla auditory nerve fibers. II. Dependence on spontaneous activity and relation to cochlear nonlinearity. *J. Neurophysiol.* 100, 2899–2906. doi: 10.1152/jn.90639.2008
- Thompson, A. M. (2000). Facilitation, augmentation and potentiation at central synapses. *Trends Neurosci.* 23, 305–312. doi: 10.1016/S0166-2236(00)01580-0
- Trussell, L. O. (2002). Modulation of transmitter release at giant synapses of the auditory system. *Curr. Opin. Neurobiol.* 12, 400–404. doi: 10.1016/S0959-4388(02)00335-5
- Turecek, R., and Trussell, L. O. (2001). Presynaptic glycine receptors enhance transmitter release at a mammalian central synapse. *Nature* 411, 587–590. doi: 10.1038/35079084
- Varela, J. A., Song, S., Turrigiano, G. G., and Nelson, S. B. (1999). Differential depression at excitatory and inhibitory synapses in visual cortex. *J. Neurosci.* 19, 4293–4304.
- Venkataraman, Y., and Bartlett, E. L. (2013). Postnatal development of synaptic properties of the GABAergic projection from inferior colliculus to auditory thalamus. *J. Neurophysiol.* 109, 2866–2882. doi: 10.1152/jn.00021.2013
- von Gersdorff, H., and Borst, J. G. G. (2002). Short-term plasticity at the calyx of Held. *Nat. Rev. Neurosci.* 3, 53–64. doi: 10.1038/nrn705
- von Gersdorff, H., and Matthews, G. (1997). Depletion and replenishment of vesicle pools at a ribbon-type synaptic terminal. *J. Neurosci.* 17, 1919–1927.
- von Gersdorff, H., Schneggenburger, R., Weis, S., and Neher, E. (1997). Presynaptic depression at a calyx synapse: the small contribution of metabotropic glutamate receptors. *J. Neurosci.* 17, 8137–8146.
- Walcher, J., Hassfurth, B., Grothe, B., and Koch, U. (2011). Comparative post-hearing development of inhibitory inputs to the lateral superior olive in gerbils and mice. *J. Neurophysiol.* 106, 1443–1453. doi: 10.1152/jn.01087.2010
- Wang, L. Y., and Kaczmarek, L. K. (1998). High-frequency firing helps replenish the readily releasable pool of synaptic vesicles. *Nature* 394, 384–388. doi: 10.1038/28645
- Wang, Y., and Manis, P. B. (2006). Temporal coding by cochlear nucleus bushy cells in DBA/2J mice with early onset hearing loss. *J. Assoc. Res. Otolaryngol.* 7, 412–424. doi: 10.1007/s10162-006-0052-9
- Wang, Y., and Manis, P. B. (2008). Short-term synaptic depression and recovery at the mature mammalian endbulb of Held synapse in mice. *J. Neurophysiol.* 100, 1255–1264. doi: 10.1152/jn.90715.2008
- Wang, Y., O'Donohue, H., and Manis, P. (2011). Short-term plasticity and auditory processing in the ventral cochlear nucleus of normal and hearing-impaired animals. *Hear. Res.* 279, 131–139. doi: 10.1016/j.heares.2011.04.018
- Wang, Y., Ren, C., and Manis, P. B. (2010). Endbulb synaptic depression within the range of presynaptic spontaneous firing and its impact on the firing reliability of cochlear nucleus bushy neurons. *Hear. Res.* 270, 101–109. doi: 10.1016/j.heares.2010.09.003
- Wojcik, S. M., Katsurabayashi, S., Guillemain, I., Friauf, E., Rosenmund, C., Brose, N., et al. (2006). A shared vesicular carrier allows synaptic corelease of GABA and glycine. *Neuron* 50, 575–587. doi: 10.1016/j.neuron.2006.04.016
- Wong, A. Y., Graham, B. P., Billups, B., and Forsythe, I. D. (2003). Distinguishing between presynaptic and postsynaptic mechanisms of short-term depression during action potential trains. *J. Neurosci.* 23, 4868–4877.
- Wu, S. H., and Kelly, J. B. (1995). Inhibition in the superior olivary complex: pharmacological evidence from mouse brain slice. *J. Neurophysiol.* 73, 256–269.
- Xu, J., and Wu, L. G. (2005). The decrease in the presynaptic calcium current is a major cause of short-term depression at a calyx-type synapse. *Neuron* 46, 633–645. doi: 10.1016/j.neuron.2005.03.024
- Yang, H., and Xu-Friedman, M. A. (2008). Relative role of different mechanisms of depression at the mouse endbulb of Held. *J. Neurophysiol.* 99, 2510–2521. doi: 10.1152/jn.01293.2007
- Yin, T. C. T. (2002). “Neural mechanisms of encoding binaural localization cues in the auditory brainstem,” in *Integrative Functions in the Mammalian Auditory Pathway*, eds Oertel, Fay, and Popper (New York, NY: Springer-Verlag), 99–159.
- Zhang, S., and Trussell, L. O. (1994). Voltage clamp analysis of excitatory synaptic transmission in the avian nucleus magnocellularis. *J. Physiol.* 480, 123–136.
- Zucker, R. S., and Regehr, W. G. (2002). Short-term synaptic plasticity. *Annu. Rev. Physiol.* 64, 355–405. doi: 10.1146/annurev.physiol.64.092501.114547

Conflict of Interest Statement: The authors declare that the research was conducted in the absence of any commercial or financial relationships that could be construed as a potential conflict of interest.

Received: 25 November 2013; accepted: 13 February 2014; published online: 10 March 2014.

Citation: Kramer F, Griesemer D, Bakker D, Brill S, Franke J, Frotscher E and Friauf E (2014) Inhibitory glycinergic neurotransmission in the mammalian auditory brainstem upon prolonged stimulation: short-term plasticity and synaptic reliability. *Front. Neural Circuits* 8:14. doi: 10.3389/fncir.2014.00014

This article was submitted to the journal *Frontiers in Neural Circuits*.

Copyright © 2014 Kramer, Griesemer, Bakker, Brill, Franke, Frotscher and Friauf. This is an open-access article distributed under the terms of the Creative Commons Attribution License (CC BY). The use, distribution or reproduction in other forums is permitted, provided the original author(s) or licensor are credited and that the original publication in this journal is cited, in accordance with accepted academic practice. No use, distribution or reproduction is permitted which does not comply with these terms.